Undercooled Phase Behind the Glass Phase with Superheated Medium-Range Order above Glass Transition Temperature

Robert Tournier, Michael I Ojovan

Undercooled Phase Behind the Glass Phase with Superheated Medium-Range Order above Glass Transition Temperature

Robert F. Tournier* (1), Michael I. Ojovan (2,3)

(1) Univ. Grenoble Alpes, CNRS, Grenoble INP, Institut Néel. 38000 Grenoble, France, *Institute of Engineering Univ. Grenoble Alpes*
(2) Department of Materials, Imperial College London, London SW7 2AZ, United Kingdom
(3) *Institute of Geology of Ore Deposits, Petrography, Mineralogy and Geochemistry (IGEM), Russian Academy of Sciences, 119017, Moscow, Russia*

e-mail of corresponding author: robert.tournier@neel.cnrs.fr

Keywords: glasses, glass transitions, percolation threshold, configuron, medium-range order

Abstract: Rapidly quenched glass formers are amorphous and transformed into glass phases by relaxing enthalpy during the first heating. Two liquids give rise, at first, to an intermediate Phase 3 below $T_3 < T_g$ respecting the entropy constraints and then, the enthalpy increases towards that of the glass phase up to T_g. The negative activation energy shows that Phase 3 is hidden behind the glassy phase acting as an intermediate invasive phase during the second cooling. Phase 3 carries a medium-range order above T_g which can be superheated above the melting temperature up to T_{n+}. The two-liquid state model predicts the thermodynamic properties as well as the relaxation times from liquids 1 to 2. The configuron model is successfully applied to 54 glasses explaining the transitions by percolation and an 'ordered' fraction equal to the critical threshold $\Phi_c = 0.15 \pm 0.01$ from T_g to T_{n+}.

Introduction

Microscopically liquids are dynamically inhomogeneous media because there is always a tendency to form microscopic metastable ordered structures whose size and lifetime grow with decreasing temperature. Thus, a liquid is homogeneous and disordered at large time and spatial scales, however it can have a short- and medium-range order locally at distances of the size of metastable clusters and over the lifetime of metastable formations [1]. Typical examples of this ordering are tetrahedral structures in silica and icosahedral structures in metallic glasses [2,3]. Local ordering in liquids is confirmed by Fischer clusters, which are associated with long-wavelength density fluctuations and revealed in glass-forming liquids and polymers [4]. Bakai has shown that density fluctuations have correlation lengths of up to 300 nm and proved to be fractal with the dimension $D < 3$ [5]. These fluctuations result from domain aggregation and their lifetime is close to the α relaxation time. A tendency to ordering is also observed in liquids above the melting temperature (liquidus). An analysis of the atomic structure of melts of simple metals demonstrates that the dense part of the liquid in molecular-dynamic models represents branched chains of almost regular tetrahedra linked in pairs by faces. The resulting clusters are fractal with the dimension $D = 2.6$ [6]. These observations are in contradiction with the commonly accepted notions that the structure of a liquid above the liquidus temperature is completely disordered and has neither long-range nor middle-range order. However, experimental observations confirm the occurrence of local ordering in liquids [7-9]. For example, ordered structures possessing the effect of remembering the thermal evolution of the melt state were found above the liquidus in glass-forming melts of silicate systems [10].

A supercooled liquid undergoes a glass transition after reheating the quenched melt. The knowledge of the melt state after quenching from temperatures higher than the melting temperature T_m is important to understand the phase transformations occurring during heating. There are two main views in the literature. The melt may be frozen in an amorphous state after quenching in the absence of thermodynamic transition at the freezing temperature T_g or may undergo a true phase transition at T_g leading to a glass state of the melt. It is considered [11,12], in contradiction with many experiments, that a melt does not contain any intrinsic nucleus above T_m as shown by the classical nucleation equation. Consequently, melts are not highly superheated above T_m before quenching despite of numerous experiments showing the existence of growth nuclei far above T_m [8]. Medium-range order of melts

exists in glass-forming liquids heated above T_m, after cooling far below T_g, in contradiction with the classical nucleation equation [10,13-15]. This equation, when completed and applied to liquids 1 and 2, predicts the formation of stable superclusters and the existence of a melting temperature of liquid "order" at $T = T_{n+}$ [16]. Superheating above T_{n+} melts this medium-range order induced after quenching giving rise to short-range order and individual superclusters only containing few atoms which disappear at much higher temperatures than T_{n+} [17]. Consequently, rapid quenching of the melt from $T > T_{n+}$ or atom deposition on substrate cooled at low temperature leads to an amorphous instead of a glass state [18] due to an absence of superclusters acting as building bricks of the glass phase.

The glass phase is created by recovering enthalpy during reheating the amorphous state up to T_g [19-22]. A liquid medium-range order is maintained after heating from T_g to T_{n+} and disappears above T_{n+} [13,22]. The medium-range order may come back after cooling at a second temperature $T_{n+} < T_m$, symmetrical of the first T_{n+} regarding to T_m because the new superclusters grow around the residual nuclei surviving above $T_{n+} > T_m$ [13,17]. Reheating a glass up to a temperature T respecting $T_m < T < T_{n+}$ does not melt the medium-range order and directly leads by cooling to a glass phase characterized by an entropy higher than $-S_m$ the crystal entropy with the entropy origin fixed at T_m.

The amorphous state obtained after hyper-quenching does not respect the Kauzmann's entropy constraint [18-24]. Superclusters and the glass phase are built by reheating the amorphous liquid from a nucleation temperature T_{n-} far below T_g and up to a second homogeneous nucleation temperature $T_{n-} = T_g$ with formation of a new phase called Phase 3 respecting the Kauzmann constraints [13,16]. The thermodynamic parameters of this new supercooled phase are obtained in a model involving two liquid states separated by their Gibbs free energy difference determined from the value of T_g [23,25,26]. This model has some analogy with the concept of two liquids applied to supercooled water transformations [27]. Desgranges and Delhommelle show that methanol under shear also reveals the existence of liquid polymorphism in this system driven out-of-equilibrium by undercooling [28] and that liquid polymorphs play a pivotal role during the crystallization of silicon. This implies that, theories, like the classical nucleation theory, should be modified to account for the role of liquid polymorphs in the nucleation process [29]. A two-liquid model describes the supercooled water as a glacial phase. These two liquids give rise to a third liquid called Phase 3 having a Gibbs free energy equal to the difference of their own Gibbs free energies, a glass transition at T_g, and a medium range order up to T_{n+}. The completed classical nucleation equation predicts the Phase 3 transformation in glacial phases of supercooled water, triphenyl phosphite, n-butanol, and d-mannitol in perfect quantitative agreement with experiments just knowing the initial value of their T_g before transformation in glacial phases [13,16].

The phase transition assumption viewed as a percolation phenomenon at T_g is examined using all the thermodynamic parameters accumulated in many publications. Wool et al shows that the liquid-to-glass transformation results from percolation phenomenon of atom groups formed above T_g during cooling [30-32]. Angell and Rao's congruent bond lattice model of topologically disordered oxide systems analyze the connectivity of disordered systems accounting for the threshold degree Φ of connectivity [33]. Ojovan et al treat the liquid–glass transition during heating as a percolation phase transition in the system of broken bonds called configurons [34-36]. The critical density is evaluated from Scher-Zallen's predictions leading to $\Phi = 0.15 \pm 1$ at T_g [37]. They still predict that the first sharp diffraction minimum in the pair distribution function is expected to contain information on structural changes in amorphous materials at T_g and T_{n+} [38]. Moreover, the configuron percolation theory naturally treats the known behavior of heat capacity which drops continuously on cooling of melts and diverges i.e. it is seen as a very sharp and narrow peak at T_g on heating of glasses evidencing the phase transformation as due to configuron association in macroscopic percolating clusters.
The work developed here is devoted to Phase 3 and configurons. For that purpose, several methods are successively used without forgetting Souletie and Tholence's conclusion that the power law gives a better account of the available experimental evidence than the Vogel-Fulcher-Tammann law [39]. One method is based on previous studies of Rammal and Benoit and Henley devoted to spin glasses predicting that the relaxation time $\tau/\tau_0 \sim \exp(W/T)$ increases with $W \sim \ln\xi$ where ξ is the coherence length of percolating clusters [40,41]. The energy W also contains the delocalization energy Δe_e of atoms calculated by Sanditov, Ojovan and Darmaev which is related to the ultimate displacement of a bridging atom at T_g and above T_g [42]. This occurs when the energy of thermal vibrations of the lattice per atom

becomes equal or lower than Δe_e. The value of Δe_e is deduced from the contribution of $D^*T^2/(T-T_0)^2$ to $\ln(\tau/\tau_0)$ where T_0 is predicted with a thermodynamic law from the knowledge of T_g instead of being measured [26]. The delocalization energy, proportional to the temperature T, varies as $\ln\xi$ in a wide range of temperatures when the Vogel-Fulcher-Tammann (VFT) law is used for fragile liquids. This VFT law only works at T_g for strong liquids. These observations confirm that Ln (ξ^ν) is equal to νLn (1-T_g/T) without confirmation of an exponent ν which could be equal to -0.88. A critical temperature $T_c < T_g$ was proposed in few glasses by Souletie in 1990 claiming that T_c could be determined by extrapolating to zero the reverse of d(logT)/d(logη) versus T (K) where η is the viscosity or by plotting log(η) versus log(ξ) [(43)]. He found T_c = 568 K with T_g = 637 K [44] for $Pd_{77.5}Cu_6Si_{16.5}$ in agreement with the value of T_3 = 572 K predicted in this paper, T_c = 169 K for T_g = 190 K for glycerol in agreement with Birge and Nagel predictions and T_3 = 174 K [45,46] . The existence of Phase 3 was anticipated 30 years ago using the dynamical scaling near a transition at T_c characterized by a power law for τ/τ_0 [47]. The negative activation energy E_a of Phase 3 reveals that its formation at $T_3 < T_g$ is masked during cooling by an intermediate phase acting at the temperature T_g where E_a is equal to zero. An analogous phenomenon is known in gaz-phase reactions [48].

The Gibbs free energy of "ordered" liquid phase 3 is predicted below and above T_g including the critical anomaly associated with the phase transition which has a weak contribution as shown by a very-narrow specific heat peak when it is detected around T_g [44,49-51]. The theoretical Gibbs free energy of configurons is also used and successfully introduced in that of Phase 3 [36]. It is proportional to the temperature as predicted by Sanditov et al and determine the fraction of configurons involved in kinetic units having a coherence length ratio of ξ/ξ_0 [42]. The threshold degree $\Phi \cong 0.15 \pm 0.01$ of configuron percolation involved in kinetic units associated with medium-range order in phase 3 is confirmed.

1- The glass transition temperature

1.1 Critical phenomena are observed around T_g.

Several experimental proofs exist. A critical phenomenon is observed in few measurements of heat capacity. The most spectacular peaks have been obtained by Alba et al in 1990 with molecular glasses such as toluene, m-xylene, and m-toluidine [49,50] confirmed by Wilde et al in 2004 with the bulk metallic glass $Pd_{77.5}Cu_6Si_{16.5}$ [44], Hassine et al with n-butanol and Mandanici et al with ethylcyclohexane [51,52]. As an example, the heat capacity of m-toluidine is represented in Figure 1:

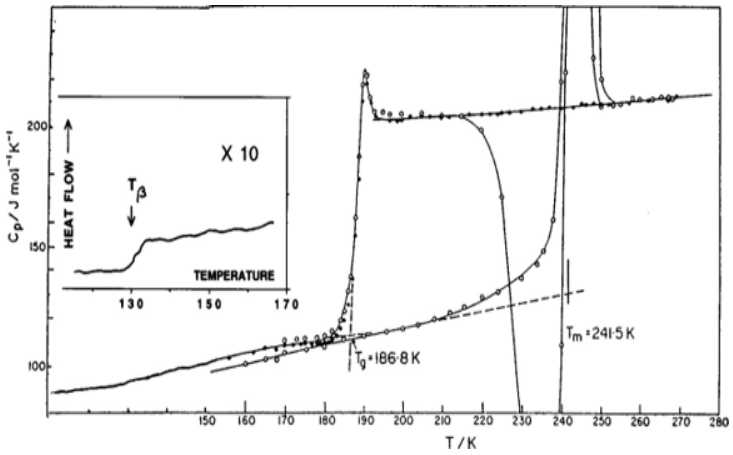

Figure 1. *Heat capacity vs temperature for liquid, glass, and crystal states of m-toluidine according to DSC measurements from [50] [C. Alba-Simonesco, J. Fan, and C.A. Angell, J. Chem. Phys.110 (1999) 5262] with permission of AIP Publishing.*

A very sharp and narrow peak is measured in Figure 1 accompanied by precursory effects below T_g. Interestingly that heat capacity behavior is characterized by a hysteresis curve - the peak is seen on heating and not seen on cooling down the material although the capacity jump is kept unchanged. In

addition, the jump at T_g covers all the difference of heat capacity between those of liquid and crystal as expected.

.

1-2 The jump of heat capacity is not always fully accomplished at T_g.

As an example, the heat capacity of 1-propanol is reproduced in Figure 2 from Takahara et al [53]

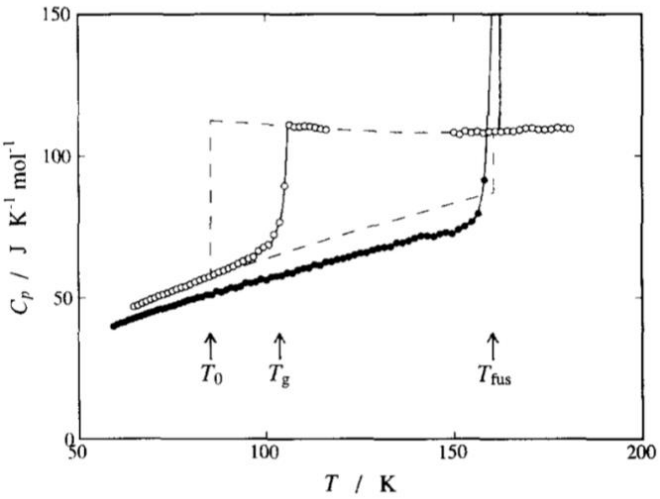

Figure 2. *Heat capacities of glassy-liquid (o) and crystalline (**o**) states of 1-propanol at 108.4 MPa. The dashed lines represent the extrapolation of the heat capacities determined by the least-squares. Reproduced from [53] [S. Takahara, O. Yamamuro, H. Suga, J. Non-Cryst. Sol. 171 (1994) 259-270].*

Many other heat capacity measurements reproduce this phenomenon without critical phenomenon [54-56]. The applied cooling rate below T_g is too high compared to the duration of the transition. A part of the sample could be frozen without contribution to the jump and to the total thermodynamic transition [57]. Thin film deposition at too low temperatures below T_g leads to a constant volume far above that of the glass state [18].

1-3 **The thermodynamic glass transition occurs at a temperature where the heat capacity difference between those of Liquid 1 and crystal becomes equal to that of Phase 3.**

The heat capacity jump is equal to $1.5 \times S_m/T_m$ in many glasses as shown in 1960 by Wunderlich [58] and confirmed for many glasses [26] (where S_m is the crystal entropy of fusion). In Figure 3, the glass transition is pushed at higher temperatures by increasing the heating rate up to a temperature where the glass formation time is equal to the heating time across the transition width. The new glass transition is accompanied by a weak latent heat as represented in Figure 3. The latent heat is equal to the surface of triangle ABC. This phenomenon is shown by heat capacity measurements at high heating rates [59]

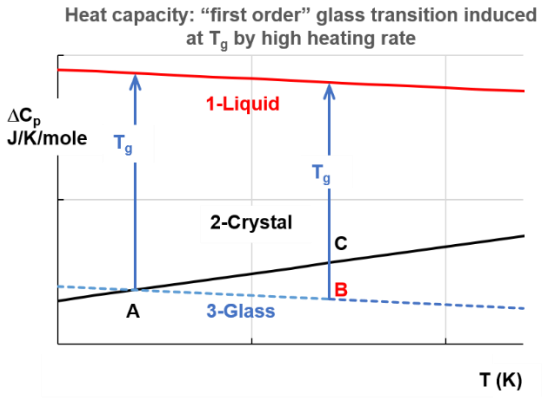

Figure 3. *The heat capacity and latent heat induced by an increase of T_g. A high heating rate increases the glass transition temperature from A to B and produces a latent heat equal to the triangle area ABC accompanying a heat capacity jump equal to 1.5×S_m.*

The latent heat coefficient Δε associated with a transition at T ≠ T_g is calculated using the following equations predicting two reduced homogeneous nucleation temperature θ_{n-} in fragile Liquid 2 resulting from the completed classical nucleation equation [13,16]:

$$\theta_{n-} = (-3 \pm [9 - 4(2 - \varepsilon_{gs0} - \Delta\varepsilon)\,\varepsilon_{gs0}/\theta_{0g}^2]^{0.5})\,\theta_{0g}^2/2\varepsilon_{gs0}\,, \quad (1)$$

where $\varepsilon_{gs}(\theta) = \varepsilon_{gs0}\left(1 - \theta^2 \times \theta_{0g}^{-2}\right) + \Delta\varepsilon$, (2)

$$\varepsilon_{gs}(\theta = 0) = \varepsilon_{gs0} = 1.5\theta_2 + 2 = 1.5\theta_g + 2, \quad (3)$$

$$\theta_{0g}^2 = \frac{8}{9}\varepsilon_{gs0} - \frac{4}{9}\varepsilon_{gs0}^2. \quad (4)$$

For a latent heat coefficient Δε = 0, $\theta_{n-} = \theta_g = (T_g\text{-}T_m)/T_m$ while there are two homogeneous nucleation temperatures θ_{n-} for the same value of Δε, one above θ_g leading to an increase of $T_g = T_{n-}$ even to glacial phase transitions for high values of Δε and a decrease symmetrical from the first one with regard to T_g. This equation leads to $\Delta\varepsilon \times H_m = 0.024 \times H_m$ for an increase of T_g of 21 K of triphenyl phosphite using a heating rate of 1000 K/s (H_m being the crystal melting heat) [13].

1-4 Thermodynamic origin of the glass transition

The glass transition is now recognized as being a thermodynamic transition instead of a liquid freezing. The glass transition is seen as a manifestation of critical slowing down near a second-order phase transition with the possible existence of several classes of universality [43]. A model predicting the specific heat jump is based on a percolation-type phase transition with the formation of dynamical fractal structures near the percolation threshold [30,31,34-36]. Macroscopic percolating clusters formed at the glass transition have been visualized [32]. High precision measurements of third- and fifth-order non-linear dielectric susceptibilities lead to a fractal dimension $d_F = 3$ for the growing transient domains [60]. An observation of the structural characteristics of medium-range order with neutrons and X-rays leads to $d_F = 2.31$ [61]. The heat capacity jump of $1.5 \times S_m$ is predicted for many liquids [62] having an enthalpy coefficient $\varepsilon_{ls}(\theta)$ for fragile Liquid 1 respecting (5-7) and a = 1:

$$\varepsilon_{ls}(\theta) = \varepsilon_{ls0}(1 - \theta^2 \times \theta_{0m}^{-2}), \quad (5)$$

$$\varepsilon_{ls}(\theta = 0) = \varepsilon_{ls0} = 1.5\theta_1 + 2 = a\theta_g + 2, \quad (6)$$

$$\theta_{0m}^2 = \frac{8}{9}\varepsilon_{ls0} - \frac{4}{9}\varepsilon_{ls0}^2. \quad (7)$$

2- The enthalpy coefficients

2-1 The enthalpy coefficients of Phase 3

New Phase 3 is viewed as having an enthalpy coefficient equal to the difference $\Delta\varepsilon_{lg}$ between those of liquids 1 and 2 and given in (8) [13,16,23]:

$$\Delta\varepsilon_{lg}(\theta) = \varepsilon_{ls} - \varepsilon_{gs} = \varepsilon_{ls0} - \varepsilon_{gs0} + \Delta\varepsilon - \theta^2\left(\varepsilon_{ls0}/\theta_{0m}^2 - \varepsilon_{gs0}/\theta_{0g}^2\right). \quad (8)$$

This phase undergoes the glass transition at T_g and obeys (8) up to the temperature T_{n+} of homogeneous nucleation respecting $\Delta\varepsilon_{lg} = \theta_{n+}$ where the liquid mean-range order is broken giving rise to short-range order inside the residual coherence length ξ_0. This enthalpy difference belongs to the Gibbs free energy

G_d of broken bonds in the configuron model. The system of bonds has two states, namely, the ground state corresponding to unbroken bonds and the excited state corresponding to broken bonds. It has been described by the statistics of two-level systems separated by the energy interval G_d. The Gibbs free energy of Phase 3 is equal to G_d with the glass phase 3 entropy equal to zero up to T_g [34-36].

2-2 The enthalpy coefficients of strong liquids 1 and 2

A strong liquid 1 has a reduced temperature $\theta_{0m} \leq -2/3$ equal to its VFT temperature determined from viscosity measurements. The VFT temperature of Liquid 2 is fixed to $T_{VFT} = 0$ K ($\theta_{0g} = -1$) because the relaxation time follows an Arrhenius law. The enthalpy coefficients are calculated from (9-10);

$$\varepsilon_{ls0} = (3\theta_g + 2)/\left(1 - {\theta_g^2}/{\theta_{0m}^2}\right), \quad (9)$$

$$\varepsilon_{gs0} = (3\theta_g + 2)/\left(1 - {\theta_g^2}/{\theta_{0g}^2}\right). \quad (10)$$

There are some cases where Liquid 1 is fragile above T_g and Liquid 2 is strong. In these conditions, θ_{0g} is equal to -2/3 and $T_{0g} = T_m/3$. This event occurs in $Mg_{69}Zn_{27}Yb_4$ and leads to a quasi-crystalline phase through a first-order transition [63] as shown in Chapter 4

3- Two examples of liquid relaxation times

3.1- Relaxation times of fragile liquids $Au_{49}Ag_{5.5}Pd_{2.3}Cu_{26.9}Si_{16.3}$ above T_g

There are two relaxation times associated with liquids 1 and 2 at each temperature. The nucleation times 1-Liq1 and 2-Liq2 are equal at T = 389 K for T_g = 377 K [64,65]:

$$Ln({\tau}/{\tau_0}) = {B_1}/{(T - T_{0m})} = {B_2}/{(T - T_{0g})} \cdot \quad (11)$$

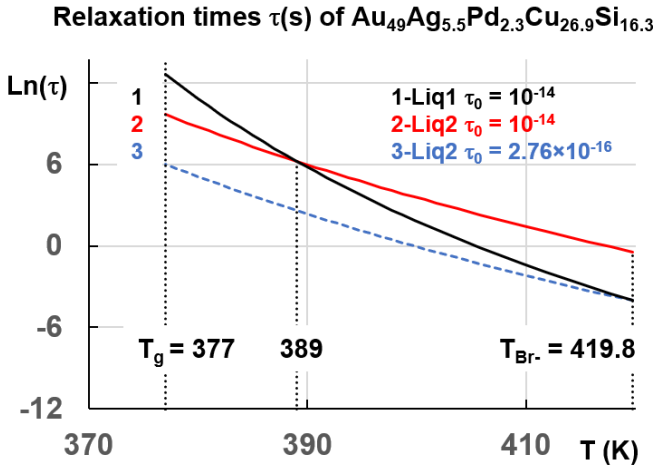

Figure 4. *Relaxation times τ of liquids $Au_{49}Ag_{5.5}Pd_{2.3}Cu_{26.9}Si_{16.3}$. 1-Liq1 obeys the first VFT law (T_{0m}, B_1) with $\tau_0 = 10^{-14}$ s. 2-Liq2 and 3-Liq2 obeys the second VFT law (T_{0g}, B_2) with $\tau_0 = 10^{-14}$ s and $\tau_0 = 2.76\times10^{-16}$ s.*

Using (3,4,6,7) with a = 1, T_m = 610 K, and T_g = 377 K, we predict the VFT laws with T_{0m} = 304.43 K, T_{0g} = 242.28 K; $B_1 = T_{0m}\times10.68$ and $B_2 = T_{0g}\times23.29$ with τ = 504 s and $\tau_0 = 10^{-14}$ s in good agreement with experiments of Gallino et al [64] and Hechler et al [65]. The relaxation times of 1-Liq1 and 3-Liq2 are equal at T_{Br-} = 419.8 K as defined by the enthalpies of liquid 1 and 2 given by (12,13) calculated with (3,4,6,7) and T_g = 377 K:

$$\varepsilon_{ls}(\theta) = 1.61803\left(1 - {\theta^2}/{0.27468}\right), \quad (12)$$

$$\varepsilon_{ls}(\theta) = 1.42705\left(1 - {\theta^2}/{0.36339}\right), \quad (13)$$

where $\varepsilon_{ls}(\theta) = \varepsilon_{gs}(\theta)$ for $\theta = \theta_{Br-} = -0.31188$.

The relaxation time 3-Liq2 is parallel to 2-Liq2 with $\tau_0 = 2.76\times10^{-16}$ s instead of 10^{-14} s because the time-lag required for an equilibrium distribution of atoms to be established during the transition from liquid 1-to-liquid 2 is much longer above than below 389 K.
A cooling rate of 5 K/min leads to an uncomplete heat capacity jump extending from 340 to 400 K [56] because the relaxation times are high in this range of temperatures as shown in Figure 4.
A much weaker cooling rate from 394 to 383 K lowers the enthalpy of Liquid 1 towards that of liquid 2. The recovered enthalpy 0.2×383 J/g-atom [65] is much smaller than the enthalpy difference between those of Liquid 1 and Liquid 2 which is equal to $\Delta\varepsilon_{lg}\times H_m = 395$ J in (14) with $H_m = 5100$ J/mole:

$$\Delta\varepsilon_{lg}(\theta) = 0.19098(1 - \theta^2 \times 10.28). \quad (14)$$

The structural changes observed by Hechler et al [65] prove the existence of two liquid phases as predicted by this two-liquid model.

3.2- Relaxation of fragile liquid $Au_{49}Ag_{5.5}Pd_{2.3}Cu_{26.9}Si_{16.3}$ after quenching

The change of properties during aging and slow heating after the first quenching has been investigated by Gallino et al. The glass transition initially equal to about 401 K [66,67] becomes equal to 377 K after storage at 290 K in a freezer and after slow heating. They also observe a heat capacity decrease of the liquid after heating above $T_g = 377$ K. This is due to a weak decrease $\Delta\varepsilon = 0.00776$ of liquid 1 enthalpy coefficient during aging because Phase 3 and glass phase are built after the first quenching and do not preexist before heating. The glass transition expected after the first quenching and during the first annealing occurs close to the Kauzmann temperature $T_{K1} = 402.5$ K of Liquid 1, T_{K1} also being the temperature where the enthalpy difference of liquids 1 and 2 would be equal to that between liquid 1 and crystal for $T_g = T_{K1}$. The enthalpy coefficients of liquids 1, 2 and 3 after classical annealing would be given in (15-17):

$$\varepsilon_{gs} = 1.48978x(1 - \theta^2/0.33783), \quad (15)$$

$$\varepsilon_{ls} = 1.65985x(1 - \theta^2/0.25093), \quad (16)$$

$$\Delta\varepsilon_{lg}(\theta) = 0.17008(1 - \theta^2 \times 12.965). \quad (17)$$

The phase 3 enthalpy coefficient given in (17) using (1) is represented in Figure 5 with the glass transition at 377 K after aging. The temperature of sample storage must be lower than the nucleation temperature $T_{n-} = 282.7$ K (deduced from (1) with $\Delta\varepsilon = \Delta\varepsilon_{lg0} = 0.17008$) to stabilize the glass transition at $T_g = 402.5$ K without relaxed enthalpy $\Delta\varepsilon\times H_m$.

A cooling rate of 5 K/min shows that the slope of ΔC_p (T) changes twice: the first time between 340 and 365 K and the second time above 385 K. It may indicate two distinctly different glass-transition processes revealed by an uncomplete glass transition [56]. These double transitions could be due to the presence of Phase 3 transition in the sample fraction which is not transformed into a glass phase at 389 K. A similar double-stage glass transition is still observed in a metallic glass [68].

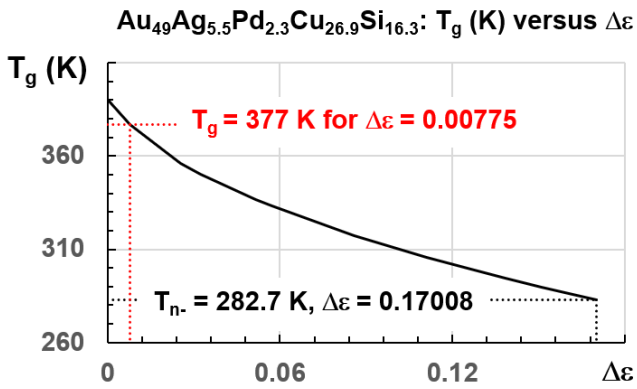

Figure 5. *The glass transition at T_g of $Au_{49}Ag_{5.5}Pd_{2.3}Cu_{26.9}Si_{16.3}$ plotted versus the relaxed-enthalpy coefficient $\Delta\varepsilon$. T_g = 377 K obtained with $\Delta\varepsilon$ = 0.00775 using (1).*

3.3- Relaxation times of liquid $Zr_{65}Cu_{27.5}Al_{7.5}$

The glass transition occurs at T = 666 K with T_m = 1180 K [69]. The heat capacity jump is equal to 1.5×S_m. The enthalpy coefficients calculated using (3,4,6,7) obey (18-20):

$$\varepsilon_{ls} = 1.5644 x(1 - \theta^2/0.30286), \quad (18)$$

$$\varepsilon_{gs} = 1.3466 x(1 - \theta^2/0.39105), \quad (19)$$

$$\Delta\varepsilon_{lg}(\theta) = 0.2178 - \theta^2 \times 1.7218. \quad (20)$$

The relaxation times are represented in Figure 6 using (11).

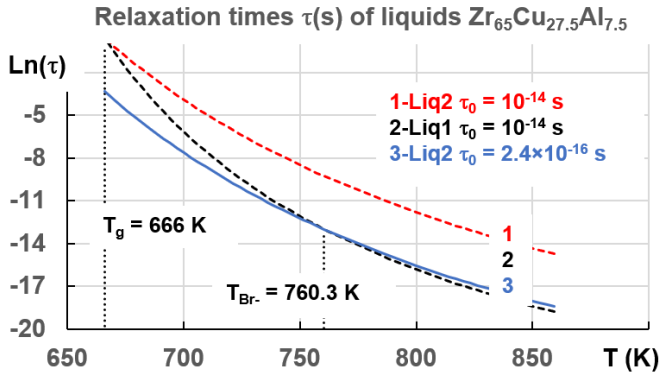

Figure 6. *Relaxation times of liquids $Zr_{65}Cu_{27.5}Al_{7.5}$. 2-Liq1 obeys the first VFT law (T_{0m}, B_1) with $\tau_0 = 10^{-14}$ s. 1-Liq2 and 3-Liq2 obeys the second VFT law (T_{0g}, B_2) with $\tau_0 = 10^{-14}$ s and $\tau_0 = 2.4\times10^{-16}$ s.*

1-Liq2 and 2-Liq1 have the same relaxation time $\tau \cong 1.5$ s at T_g using VFT laws with T_{0m} = 530.61 K, T_{0g} = 442.1 K, $B_1 = T_{0m}\times8.33$, $B_2 = T_{0g}\times16.53$, and $\tau_0 = 10^{-14}$ s in good agreement with experiments of Zhou et al [69] and Kuchemann et al [70]. The relaxation times of 2-Liq1 and 3-Liq2 are equal to 5×10^{-7} s at T_{Br-} = 760.3 K defined by the enthalpies of liquid 1 and 2 given by (18,19) calculated with (3,4,6,7) and T_g = 666 K. The glass transition temperature is expected to increase from 666 up to 760 K with a heating rate varying from 0.67 K/s to 2×10^6 K/s in perfect agreement with [70]. The latent heat coefficient $\Delta\varepsilon$ calculated with (1) at T_{Br-} = 760.3 K corresponds to 2.2% of the melting heat.

The Kauzmann temperature of Liquid 1 is much higher than T_g. The glass transition cannot occur at higher temperature because the specific heat of Phase 3 would be too weak to accommodate a glass transition at $T_{K1} = T_g$ = 778 K (θ_{K1} = -0.34).

4- A fragile-to-strong liquid transformation in $Mg_{69}Zn_{27}Yb_4$

For $Mg_{69}Zn_{27}Yb_4$, T_g is equal to 373 K, T_m to 663 K and the melting heat H_m = 7600 J/K/mole [**63**]. In Figure 7, the enthalpy coefficient of Phase 3 is plotted versus temperature. The enthalpy coefficients of liquids 1, 2 and 3 are given in (21-23) and (21) is calculated with (3,4,6,7) and a = 0.97 because liquid 1 is fragile while Liquid 2 with (22) is strong and calculated with (9) and θ_{0g}^2 = 0.44444 ($T_{0m} = T_m/3$) instead of one for other strong glasses:

$$\varepsilon_{ls} = 1.5757 x(1 - \theta^2/0.29713), \quad (21)$$

$$\varepsilon_{gs} = 1.20765 x(1 - \theta^2/0.44444), \quad (22)$$

$$\Delta\varepsilon_{lg}(\theta) = 0.36807 - \theta^2 \times 2.58584. \quad (23)$$

The enthalpy coefficient of Phase 3 is given by (23) and equal to 0.35865 at 623 K. Its enthalpy coefficient at the temperature where ε_{ls} = 0 (T_{0m} = 301.6 K, θ_{0m} =-0.5451) is -0.40027. The latent heat coefficient is expected to be -0.35865-0.40027 = -0.75982 in perfect agreement with the measured value -0.76.

This transformation temperature is predicted and expected to lead in principle to a new strong glass phase having T_g = 655.78 K as shown by (1) using (21) and $\Delta\varepsilon$ = 0.76. This temperature cannot be attained because the entropy available at this temperature is too small to accommodate the entropy increase at the phase melting. This event occurs at 623 K when the available entropy in Phase 3 with T_g = 655.78 K is equal to the entropy variation from 623 K to T_m. This new phase is quasi-crystalline [**63**] instead of being a glassy glacial phase [13]. Rapid superheating of this phase escaping from crystallization could lead to melting at $\theta_{n+} = \Delta\varepsilon_{lg}$ = 0.2306 (T_{n+} = 816 K). The missing enthalpy for crystal formation is about $0.24 \times H_m$ = 1800 J/mole in agreement with the experiments.

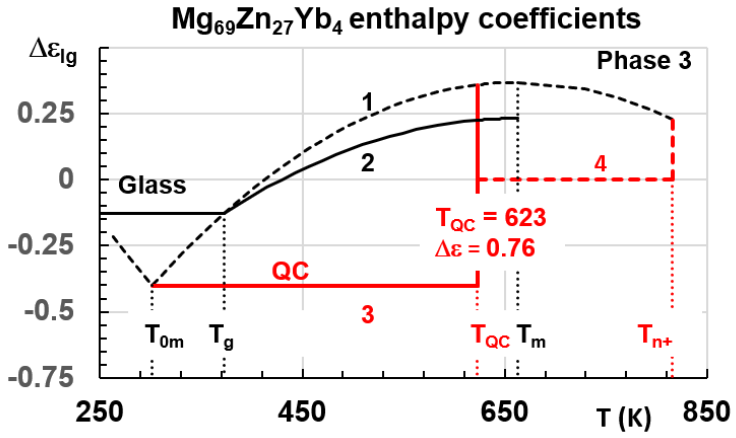

Figure 7. *The phase 3 enthalpy coefficient of $Mg_{69}Zn_{27}Yb_4$, versus T (K). 1- Enthalpy coefficient of Phase 3 for fragile liquid 1 and strong liquid 2. 2- Enthalpy coefficient for fragile liquids 1 and 2. 3- A first-order transformation predicted at 623 K with a latent heat coefficient equal to 0.75982 and to $\Delta\varepsilon_{lg}(T_{0m}) + \Delta\varepsilon_{lg}$ (623K). 4- This new QC phase expected to melt at T_{n+} = 816 K if crystallization is avoided.*

5- Entropy of fragile liquids respecting a = 1 (ΔC_p (T_g) = 1.5×S_m)

The Phase 3 and Liquid 1 entropies $S_3(T)$ and $S_1(T)$ are calculated from their heat capacity and are given in (24,25) knowing that the liquid entropy S_2 (T) is equal to the difference $S_1(T)$-$S_3(T)$:

$$S_1(T) = -2\left(\frac{\varepsilon_{ls0}}{\theta_{0m}^2}\right) S_m \frac{(T_m - T)}{T_m} + 2S_m Ln\left(\frac{T_m}{T}\right)\left(\frac{\varepsilon_{ls0}}{\theta_{0m}^2}\right), \quad (24)$$

$$S_3(T) = -2\left(\frac{\varepsilon_{ls0}}{\theta_{0m}^2} - \frac{\varepsilon_{gs0}}{\theta_{0g}^2}\right) S_m \frac{(T_m - T)}{T_m} + 2S_m\, Ln(\frac{T_m}{T})(\frac{\varepsilon_{ls0}}{\theta_{0m}^2} - \frac{\varepsilon_{gs0}}{\theta_{0g}^2}). \quad (25)$$

The quantities ε_{ls0}, ε_{gs0}, θ_{0m}^2 and θ_{0g}^2 are calculated from (3,4,6,7) for each value of θ_g and S_m and the coefficients a into (6) are equal to 1. The entropies in Figure 8 are for liquids having a heat capacity jump of $1.5S_m$ at T_g. $S_1(\theta_g)$ is minimum and equal to the crystal entropy (-1) for θ_g = -0.3402 and $S_2(\theta_g)$ for θ_g = -0.4544. $S_3(\theta_g)$ being far above its minimum value authorizes Phase 3 formation. There is no more fragile liquid for θ_g < -0.5 [62].

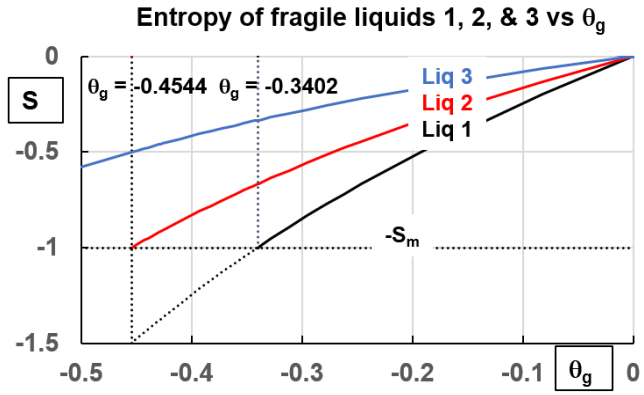

Figure 8. *Entropy of fragile liquids 1, 2, and 3 versus reduced glass transition temperature θ_g. The entropy unit is S_m. The Kauzmann temperature of liquid 1, θ_{K1} = -0.3402, that of liquid 2, θ_{K2} = -0.4544. The crystal entropy S_m = -1. Phase 3 entropy S_3 = -0.5 for θ = -0.4544.*

6- Characteristic temperatures of 50 liquids 1 and 2 with $\Delta C_p(T_g) = 1.5 \times S_m$ (a = 1)

Fifty fragile liquids [26] are characterized by ε_{ls0}, ε_{gs0}, θ_{0m}^2 and θ_{0g}^2 calculated from (3,4,6,7) for each value of θ_g. The characteristic temperatures T_g, T_m, θ_g, T_{0g}, T_{0m}, T_3 and T_{n+} are given in Table 1. The hidden transition of Phase 3 at $T_3 < T_g$ occurs at the reduced temperature θ_3 given in (26):

$$\theta_3 = -\left(\frac{\Delta\varepsilon_{lg0}}{\frac{\varepsilon_{ls0}}{\theta_{0m}^2} - \frac{\varepsilon_{gs0}}{\theta_{0g}^2}}\right)^{0.5}, \quad (26)$$

where $\Delta\varepsilon_{lg} = -\Delta\varepsilon_{lg0}$ in (8) [13]. The reduced temperature θ_{n+} is equal, above T_m, to the reduced homogeneous nucleation temperature of Phase 3 where $\theta = \Delta\varepsilon_{lg}(\theta)$ using (8) [23]. The temperatures T_{0g} and T_{0m} are determined from (3,4) and (6,7).

Table 1 Data of fragile liquids with $\Delta C_p(T_g) \cong 1.5S_m$

The following informations can be completed referring to [26].

	Materials	T_g(K)	T_m(K)	θ_g	T_{0g}	T_{0m}(K)	$\Delta\varepsilon_{lg0}$	T_3(K)	T_{n+}(K)	Ref.
	Molecular glasses									
1	β-D-fructose	286	378	-0.24339	183	213	0.12169	271.8	414	[71-73]
2	Probucol	295	399	-0.26065	188	220	0.13033	278.9	439	[54,74,75]
3	Griseofulvin	364	493	-0.26166	232	271	0.13083	344.0	543	[74,75]
4	D-glucose	309	420	-0.26429	197	230	0.13214	291.8	463	[71-73,76]
5	1,3,5-tri-a-Naphtylbenzene	340	475	-0.28421	216	254	0.14211	319.1	527	[76,77]
6	Phenobarbital	319	447	-0.28635	202	238	0.14318	299.2	497	[74,75]
7	Isopropyl benzene	125	177	-0.29379	79	93	0.14689	117.0	197	[78]
8	Hydro-chloro-thiazide	385	547	-0.29616	244	288	0.14808	359.9	610	[74,75]
9	3-Methylpentane	77	110	-0.30000	49	58	0.15000	71.9	123	[53,79]

10	m-Cresol	199	286	-0.30420	126	149	0.15210	185.5	320	[49,50]
11	Xylitol	244	358	-0.31844	154	183	0.15922	226.4	402	[80]
12	Phenolphthalein	363	533	-0.31895	230	273	0.15947	336.7	599	[71,76]
13	9-Bromophenanthrene	225	331	-0.32024	142	169	0.16012	208.6	372	[81]
14	α-Phenyl -O-cresol	220	328	-0.32927	139	166	0.16463	203.3	370	[82]
15	H_2SO_4-3H_2O	158	237	-0.33333	100	119	0.16667	145.8	268	[71,83,84]
16	Diethylphthalate	178	267	-0.33333	113	134	0.16667	164.2	301	[85]
17	m-Fluorotoluene	123	184	-0.33152	78	93	0.16576	113.6	208	[49,50,86]
18	2-methyl tetrahydrofuran	91	137	-0.33577	58	69	0.16788	83.9	155	[87,88]
19	n-Butene	58	88	-0.34091	37	44	0.17045	53.4	100	[89,90]
20	Toluene	117	178	-0.34270	74	89	0.17135	107.6	202	[24,49,50,91]
21	Glycerol	190	292	-0.34932	121	144	0.17466	174.2	332	[71,81]
22	2-Methylpentane	78	120	-0.35000	50	59	0.17500	71.5	136	[71,92]
23	Ethylbenzene	114.5	178.1	-0.35710	73	87	0.17855	104.7	203	[18,91]
24	n-Propanol	96	150	-0.36000	61	73	0.18000	87.6	171	[53,93,94]
25	3-Bromopentane	106	167	-0.36527	68	81	0.18263	96.6	191	[87]
26	$CaAl_2Si_2O_8$	1160	1830	-0.36612	741	886	0.18306	1056.4	2090	[95-97]
27	2-methyl-1-propanol	107	172	-0.37791	69	82	0.18895	96.9	197	[94]
28	Selenium	309	494	-0.37449	198	237	0.18725	280.4	566	[98,99]
29	$CaMgSi_2O_6$	1005	1665	-0.39640	650	780	0.19820	902.9	1921	[95,100]
30	Butyronitrile	97	161	-0.39752	63	75	0.19876	87.1	186	[101,102]
31	cis-/trans-Decalin	137	231	-0.40693	89	107	0.20346	122.5	267	[81,86]
32	Ethanol	94	160	-0.41250	61	74	0.20625	83.8	186	[76,86,103-105]
33	Methanol	100	172	-0.41860	66	79	0.20930	88.9	200	[71,76]
34	Ethylene glycol	151	260	-0.41923	99	119	0.20962	134.1	302	[71,104]
35	m-Xylene	126	225	-0.44000	84	101	0.22000	110.7	263	[49,50]
	Bulk metallic glasses									
36	$Pd_{40}Ni_{10}Cu_{30}P_{20}$	578	798	-0.27569	367	431	0.13784	544.0	883	[106,107]
37	$Pd_{43}Ni_{10}Cu_{27}P_{20}$	576	802	-0.28180	365	430	0.14090	541.0	890	[57,108]
38	$Au_{49}Ag_{5.5}Pd_{2.3}Cu_{26.9}Si_{16.3}$	402.5	610	-0.34016	255	304	0.17008	370.4	690	[64-67]
39	$Pd_{40}Ni_{40}P_{20}$	582	884	-0.34163	369	440	0.17081	535.3	1001	[109]
40	$Pt_{57.3}Cu_{14.6}Ni_{5.3}P_{22.8}$	509	820	-0.37927	327	391	0.18963	460.9	940	[110]
41	$Zr_{46}Cu_{46}A_{l8}$	715	1163	-0.38521	460	552	0.19261	645.7	1337	[69-70]
42	$Zr_{58.5}Cu1_{5.6}Ni_{12.8}Al_{10.3}Nb_{2.8}$	675	1110	-0.39189	436	523	0.19595	607.7	1279	[14,110,111]
43	$Pd_{77.5}Cu_6Si_{16.5}$	637	1056	-0.39678	412	495	0.19839	572.2	1218	[43,44,112]
44	$Zr_{45}Cu_{39.3}$ $Al_7Ag_{8.7}$	691	1148	-0.39808	448	537	0.19904	620.3	1325	[113,114]
45	$Cu_{47}Ti_{34}Zr_{11}Ni_8$	673	1128	-0.40337	437	525	0.20168	602.6	1304	[115-116]
46	$Mg_{65}Cu_{25}Y_{10}$	428	739	-0.42084	281	337	0.21042	379.9	859	[117]
47	$Zr_{65}Cu_{17.5}Ni_{10}Al_{7.5}$	657	1145	-0.42620	433	520	0.21310	581.5	1334	[55,118]
48	$La_{55}Al_{25}Ni_5Cu_{10}Co_5$	466	822	-0.43309	309	371	0.21655	410.9	960	[119,120]
49	$Zr_{65}Cu_{27.5}Al_{7.5}$	666	1180	-0.43559	442	531	0.21780	586.5	1379	[69,70]
50	$La_{55}Al_{25}Ni_{10}Cu_{10}$	467	835	-0.44072	311	374	0.22036	410.1	978	[119,120]

Table 2. Strong liquids data

These data are based on the following works [26]: SiO_2 [95,121], GeO_2 [76,121,122], N-butanol [123-125], and BeF_2 [51,76,86,126].

		SiO_2	GeO_2	N-butanol	BeF_2
1	N	3	3	15	3
2	T_g	1473	830	111	590
3	T_m	1996	1388	184	825
4	H_m (J/mole)	9000	16700	9280	4770
5	θ_g	-0.26202	-0.40202	-0.39674	-0.28485

6	ε_{ls0}	1.39096	1.0182	1.14756	1.32078
7	ε_{gs0}	1.30342	0.947	0.96105	1.2466
8	$\Delta\varepsilon_{lg0}$	0.08754	0.0712	0.18651	0.074179
9	T_{0g}	0	0	0	0
10	T_{0m}	530	199	51.9	180
11	$\theta_{0m}{}^2$	0.53945	0.73381	0.51546	0.61124
12	θ_3	-0.38397	-0.62092	-0.58804	-0.42025
13	T_3	1256	599	84.1	493
14	θ_{n+}	0.07948	0.0691	0.15579	0.06973
15	T_{n+}	2154.6	1483.9	212.7	882.5
16	x_3	0.03709	0.0993	1.0812	0.04159
17	x_3/N	0.01236	0.0331	0.07208	0.013863
18	B_2	53080	29900	4000	21255
19	B_1	33980	22730	2129	14770
20	Δe_2 (J/g.atom)	441307	248589	33256	176714
21	$\Delta\varepsilon_1$ (J/g.atom)	689311	326969	62431	254289
22	i_1	112.5	94.8	135.3	103.7
23	i_2	72.07	72.05	72.07	72.05
24	i_3	40.4	22.8	63.2	31.7
25	ξ/ξ_0	2.75	2.06	1.91	2.64

The reduced melting temperature θ_{n+} of medium-range order (phase 3) is plotted in Figure 9 as a function of the reduced glass temperature and obeys (27) [23]:

$$\theta_{n+} = -0.38742 \times \theta_g \,. \qquad (27)$$

The average value of $\Delta\varepsilon_{lg}$ at this temperature is 0.13746 for fragile liquids and corresponds to a volume fraction of ordered phase given by the critical threshold equal to 0.15 ± 0.01 (see chapter 9). For the strong liquids, the average is 0.0728 for SiO2, GeO_2 and BeF_2 indicating that their kinetic entities have a lower enthalpy for the same critical volume fraction.

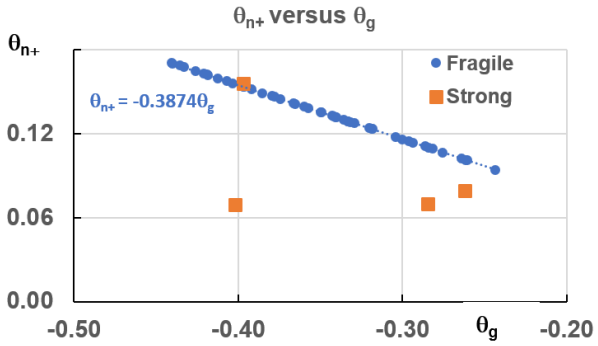

Figure 9. *The reduced melting temperature $\theta_{n+} = \Delta\varepsilon_{lg}(\theta_{n+})$ of Phase 3 medium-range order versus θ_g for 50 fragile liquids and for 4 strong liquids.*

7- Activation energy and atom delocalization energy Δe (J/g-atom)

7-1 Equations

The relaxation time is viewed as being temperature dependent through a VFT law given in (28):

$$Ln(\tau/\tau_0) = B/(T - T_0) = D^*T_0/(T - T_0). \quad (28)$$

The VFT temperatures T_0 of liquids 2 and 1 are T_{0g} and T_{0m} given by (4,7). The parameters B are determined to lead to τ values of 44-45 s with $\tau_0 = 10^{-14}$ s when (28) is applied.

The activation energies of liquids 1, 2 called W_1 and W_2 are given in (29,30)

$$W_1 = B_1RT/(T - T_{0m}), \quad (29)$$

$$W_2 = B_2RT/(T - T_{0g}). \quad (30)$$

The difference W_3 between W_1 and W_2 in (31) corresponds to the activation energy of Phase 3:

$$W_3 = B_1RT/(T - T_{0m}) - B_2RT/(T - T_{0g}), \quad (31)$$

B_1 and B_2 are determined from a relaxation time of 44-45 s in Table 2 at T_g.

The difference between an Arrhenius law (W/T) and a VFT law ($B/(T-T_0)$ is w/T for liquids 1 and 2 as defined in (33)

$$B/(T - T_0) = W/RT - w/RT, \quad (33)$$

where W and w are constants at each temperature. This gap is considered as due to the bonds which are broken or built at the temperature T in the formation model of moving entities. The change of Arrhenius law appears in the derivative of this relation as already shown with other phenomenological laws for the viscosity [34,35,42]:

$$-B/(T - T_0)^2 = -W/RT^2 + w/RT^2. \quad (34)$$

The delocalization energies Δe_1 and Δe_2 (J/g-atom) during heating in liquids 1 and 2 are:

$$\Delta e_1 = RB_1T^2/(T - T_{0m})^2 \quad (36)$$

$$\Delta e_2 = RB_2T^2/(T - T_{0g})^2. \quad (37)$$

The delocalization energy Δe_3 (J/g-atom) during heating in Phase 3 is:

$$\Delta e_3 = \Delta e_1 - \Delta e_2. \quad (38)$$

The energy Δe_3 in (39) is used to calculate the number i of freedom degrees of kinetic units associated with heating at T_g [42]:

$$i = 2\Delta e_3/RT, \quad (39)$$

where Δe_3 is the delocalization energy per mole of atoms in the melt. The theoretical values of i given in Table 2 are the upper limits predicted by VFT laws at T_g.

7-2 The atom delocalization energy and the number of freedoms degrees

Values of Δe_1, Δe_2 and Δe_3 and i are given in J/g-atom for many fragile glass-forming melts in Table 3 for which the specific heat jump is equal to $1.5 \times S_m$.

Table 3. Materials data used in and resulting from calculations

*	Materials	B_2	B_1	Δe_2	Δe_1	Δe_3	i_1	i_2	i_3	θ_{n+}	ξ/ξ_0
1	b-D-fructose	**3700**	2622	238612	336691	69520	283.2	200.7	82.5	0.09429	2.81

2	Probucol	**3855**	2706	243716	347101.4	72641	283.0	198.7	84.3	0.10098	2.66
3	Griseofulvin	**4758**	3338	300511	428235.4	89686	283.0	198.6	84.4	0.10137	2.66
4	D-glucose	**4045**	2834	254859	363764.5	76300	283.2	198.4	84.8	0.10239	2.63
5	1,3,5-tri-a-Naphtylbenzene	**4480**	3104	278346	402111	85492	284.5	196.9	87.6	0.11011	2.49
6	Phenobarbital	**4206**	2910	261051	377564.3	80438	284.7	196.9	87.9	0.11094	2.47
7	Isopropyl benzene	**1651**	1137	102174	148379.3	31840	285.6	196.6	88.9	0.11382	2.42
8	Hydro-chloro-thiazide	**5087**	3496	314593	457469.3	98392	285.8	196.6	89.3	0.11474	2.41
9	3-Methylpentane	**1017.5**	698	62868	91699.37	19741	286.5	196.4	90.1	0.11623	2.38
10	m-Cresol	**2630**	1799	162454	237466	51311	287.1	196.4	90.7	0.11785	2.36
11	Xylitol	**3225**	2185	199200	294057.6	64238	289.9	196.4	93.5	0.12337	2.27
12	Phenolphthalein	**4797**	3250	296324	437733.2	95562	290.1	196.4	93.7	0.12357	2.27
13	9-Bromophenanthrene	**2973**	2012	183695	271541.2	59378	290.3	196.4	93.9	0.12407	2.26
14	a-Phenil -cresol	**2904**	1952	179903	267532	58976	292.5	196.7	95.8	0.12757	2.21
15	H2SO4-3H2O	**2084**	1397	129326	192935.9	42633	293.7	196.9	96.8	0.12914	2.19
16	Diethylphthalate	**2347**	1574	145647	217380.9	47970	293.8	196.8	96.9	0.12914	2.19
17	m-Fluorotoluene	**1623**	1089	100636	149878.9	33111	293.1	196.8	96.3	0.12844	2.20
18	2-methyl tetrahydrofuran	**1199.5**	803	74525	111363.5	24666	294.4	197.0	97.4	0.13008	2.18
19	n-Butene	**763.3**	509	47563	71350.01	15865	295.9	197.3	98.7	0.13208	2.16
20	Toluene	**1539**	1025	96008	144255	32096	296.6	197.4	99.2	0.13277	2.15
21	Glycerol	**2493**	1651	156272	236025.9	52780	298.8	197.9	101.0	0.13533	2.12
22	2-Methylpentane	**1023**	677	64161	96942.77	21701	299.0	197.9	101.1	0.13560	2.11
23	Ethylbenzene	**1486**	971	94485	143592.1	33023	301.7	198.5	103.2	0.13852	2.08
24	n-Propanol	**1253.5**	823	79345	120908.1	27250	303.0	198.8	104.1	0.13947	2.07
25	3-Bromopentane	**1380**	902	87855	134484.4	30431	305.2	199.4	105.8	0.14151	2.04
26	CaAl2Si2O8	**15093**	9860	961819	1473715	333479	305.6	199.5	106.2	0.14184	2.04
27	2-methyl-1-propanol	**1382**	893	89435	138456.7	31645	311.3	201.1	110.2	0.14641	1.99
28	Selenium	**3992**	2582	257555	397441.8	91130	309.4	200.5	108.9	0.14606	1.99
29	CaMgSi2O6	**12780**	8105	853041	1344574	312048	321.8	204.2	117.7	0.15357	1.92
30	Butyronitrile	**1232**	781	82411	130117.3	30182	322.7	204.4	118.3	0.15401	1.91
31	cis-/trans-Decalin	**1723**	1081	117522	187517.5	43789	329.3	206.4	122.9	0.15765	1.88
32	Ethanol	**1175**	732	81169	130270.8	30603	333.4	207.7	125.7	0.15981	1.86
33	Methanol	**1240.5**	767	86987	140672.9	33182	338.4	209.3	129.1	0.16218	1.84
34	Ethylene glycol	**1872**	1157	131480	212788.2	50218	339.0	209.5	129.5	0.16242	1.84
35	m-Xylene	**1516**	910	113092	188121.8	45177	359.2	215.9	143.2	0.17046	1.77
	BMG										
36	**$Pd_{40}Ni_{10}Cu_{30}P_{20}$**	**7600**	5288	474571	681561.7	144370	283.7	197.5	86.1	0.10681	2.55
37	**$Pd_{43}Ni_{10}Cu_{27}P_{20}$**	**7585**	5262	471865	680569.9	144514	284.2	197.1	87.2	0.10917	2.50
38	**$Au_{49}Ag_{5.5}Pd_{2.3}Cu_{26.9}Si_{16.3}$**	**5328**	3565	330040	499229.6	108564	298.4	197.3	101.1	0.13179	2.16
39	**$Pd_{40}Ni_{40}P_{20}$**	**7656**	5102	477275	716716.3	159216	296.2	197.3	99.0	0.13274	2.15
40	**$Pt_{57.3}Cu_{14.6}Ni_{5.3}P_{22.8}$**	**6565**	4238	425693	660081.1	150889	312.0	201.2	110.8	0.14924	1.99
41	**Zr46Cu46Al8**	**9180**	5890	600764	936502.1	215306	315.1	202.1	113.0	0.15183	1.96
42	**$Zr_{58.5}Cu_{15.6}Ni_{12.8}Al_{10.3}Nb_{2.8}$**	**8620**	5493	570589	895282.7	206987	319.1	203.3	115.7	0.15372	1.94
43	**$Pd_{77.5}Cu_{6}Si_{16.5}$**	**8095**	5135	540724	853184.9	197720	322.2	204.2	118.0	0.15423	1.92
44	**$Zr_{45}Cu_{39.3}Al_{7}Ag_{8.7}$**	**8771**	5555	587361	927864.8	215364	323.0	204.5	118.5	0.15627	1.91

45	$Cu_{47}Ti_{34}Zr_{11}Ni_8$	**8498**	5350	575213	913670.5	213082	326.6	205.6	121.0	0.16304	1.89
46	$Mg_{65}Cu_{25}Y_{10}$	**5295**	3265	373446	605414.2	143172	340.3	209.9	130.4	0.16512	1.83
47	$Zr_{65}Cu_{17.5}Ni_{10}Al_{7.5}$	**8068**	4943	577316	942827.2	223614	345.2	211.4	133.8	0.16779	1.82
48	$La_{55}Al_{25}Ni_5Cu_{10}Co_5$	**5665**	3439	413545	681761.2	162498	351.9	213.5	138.5	0.16876	1.79
49	$Zr_{65}Cu_{27.5}Al_{7.5}$	**8065**	4878	593270	981345.2	234439	354.5	214.3	140.2	0.17074	1.79
50	$La_{55}Al_{25}Ni_{10}Cu_{10}$	**5610**	3368	419486	699075.4	167645	360.1	216.1	144.0	0.18424	1.77

7-3 The negative activation energy of Phase 3 in melts

Phase 3 is formed from Liquid 1 and vitrified by heating the quenched amorphous liquid up to T_3, relaxing an enthalpy equal to $\Delta\varepsilon_{lg0}H_m$ and forming two liquids. The transition at T_3 is viewed as resulting of the formation of broken bonds before attaining the formation temperature of the glass phase at T_g during the first heating. The glass phase appears as being an intermediate between Phase 3 and liquid during the second cooling. This phenomenon is known in chemistry and characterized by a transition from a positive to a negative activation energy [48]. The occurrence of negative activation energies in gas-phase reactions is explained as being due to the formation of an intermediate complex. Here, the reactants are Liquids 1 and 2, Phase 3 being the product and the glass being the intermediate. We learn from this work that the activation energy equal to zero at T_g results from the difference between the average energy of the transition state and the delocalization energy Δe_3 at T_g. This property is used to calculate the delocalization energy above T_g.

The quantities W_3/RT of five phases 3 are plotted as a function of temperature in Figure 10 for 1-ethylbenzene, 2- $Au_{49}Ag_{5.5}Pd_{2.3}Cu_{26.9}Si_{13.3}$, 3- $Pd_{43}Ni_{10}Cu_{27}P_{20}$, 4- $Pd_{77.5}Cu_6Si_{16.5.}$, 5- $Zr_{65}Cu_{27.5}Al_{7.5.}$ They are equal to zero at T_a. The characteristic temperatures T_g, T_3 and T_a of these materials and of SiO_2 are given in Table 4. The glass transition occurs at the temperature T_a for 1, 2, 3, 5 and SiO_2 and at a lower temperature for $Pd_{77.5}Cu_6Si_{16.5}$. This could also explain why the glass heat capacity is often higher that of crystal below T_g. The slopes $(dW_3/dT)_{Ta}$ in J/K are used to calculate i for temperatures above and close to T_g with (33) and they still work at temperatures very close to T_g. These values of i are the same than those presented in Tables 2 and 3 using Δe_3.

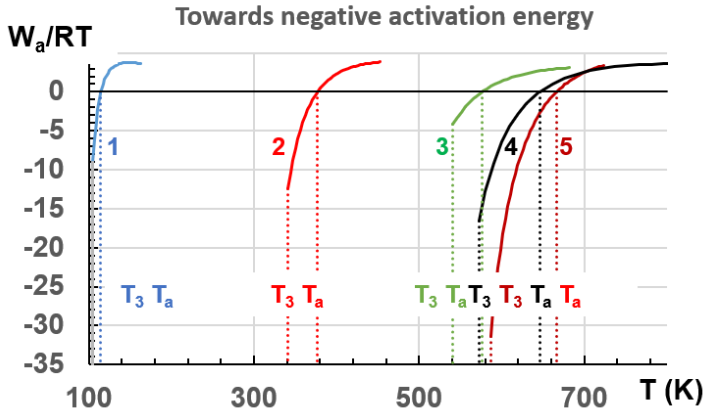

Figure 10. *The phase 3 activation energy $W_a/RT = W_3/RT$ plotted versus T (K). Negative activation energy at the temperature T_3 of Phase 3 formation. Activation energy equal to zero at T_g for the glassy intermediate phase: 1, 2, 3, and 5. 1-ethylbenzene, 2- $Au_{49}Ag_{5.5}Pd_{2.3}Cu_{26.9}Si_{13.3}$, 3- $Pd_{43}Ni_{10}Cu_{27}P_{20}$, 4- $Pd_{77.5}Cu_6Si_{16.5.}$, 5- $Zr_{65}Cu_{27.5}Al_{7.5.}$*

Table 4. Characteristic temperatures and enthalpy data

	Material	T_g (K)	T_3(K)	T_a(K)	$(dW_a/dT)_{Ta}$ (J/K/g-atom)	i ($T \cong T_g$)	$\Delta\varepsilon_{lg0}H_m/N$ (J/g-atom))
1	Ethylbenzene	114.5	105	114.5	429.6	103.3	91
2	$Au_{49}Ag_{5.5}Pd_{2.3}Cu_{26.9}Si_{16.3}$	377	370	377	464.3	111.7	974
3	$Pd_{43}Ni_{10}Cu_{27}P2_0$	576	541	576	362	87.1	966
4	$Pd_{7.5}Cu_6Si_{16.5}$	637	572	646.2	421.8	101.5	1696
5	$Zr_{65}Cu_{27.5}Al_{7.5}$	666	587	666.1	581.7	139.9	2723
6	SiO_2	1473	1256	1473	168.4	40.5	197

The numbers i determined by the VFT laws used in (32) and applied above T_g are already high because these numbers associated with kinetic entities are diverging when the temperature tends to T_g and are expected to be infinite with power laws.

8- The dynamic scaling near a phase transition using VFT laws

The standard statement near a transition at T_c is the power law given in (40) for the relaxation time [47]:

$$\tau/\tau_0 = (\xi/\xi_0)^z = (1 - T_c/T)^{-z\nu} \ , \qquad (40)$$

where ν is the coherence length exponent which is expected to be equal to 0.88 [(36)]. The coherence length diverges at the transition temperature for a percolation phenomenon and the exponent z is much higher than ν [43]. The divergences of the delocalization energies Δe_1 and Δe_2 of liquids 1 and 2 in ethylbenzene are searched near T_3 and T_g in Figure 11 using (36,37). The lines y_1 and y_2 are plotted versus x_1 = Ln(1-104.66/T) and x_2 = Ln(1-114.5/T) respectively following the scaling versus Ln(ξ) proposed for percolation phenomena in spin glasses [40,41]. These representations using VFT laws work for 107 K < T < 136 K and 121 K < T < 202.7 K respectively. The exponent value ν cannot be confirmed. The ratio B_2/T_g is expected to be equal to zν [43]; zν ≅ 13 for the average value in molecular liquids, and 12.7 for metallic glasses while B_1/T_3 is equal to an average value zν ≅ 9.4 for molecular liquids, and 9 for metallic glasses. Ratios ξ/ξ_0 are predicted in Table 3 at the melting temperature T_{n+} of medium-range order applying (40) for $T_c/T = T_g/T_{n+}$. Its average value is 2 for BMG and 2.2 for molecular liquids. These values lead to ratios ξ/ξ_0 varying from 135 to 2 and 148.5 to 2.2 when the temperature increases from T_g = 114.5 to 202.74 K while the energy Δe_3 is decreased from $429.6T_g$ to $24.5T_{n+}$. The divergence of ξ/ξ_0 towards infinite cannot be attained with VFT laws.

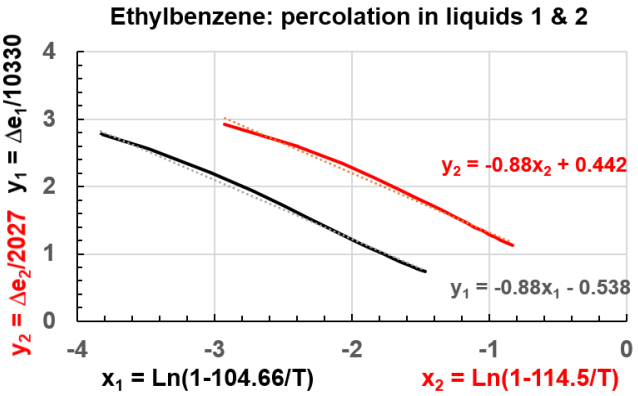

Figure 11. *Atom delocalization energy Δe_1 and Δe_2 in liquids 1 and 2 versus x_1 = Ln(1-104.66/T) and x_2 = Ln(1-114.5/T). Δe_1 and Δe_2 are reduced multiplying them by a numerical coefficient to obtain ν = -0.88. Temperature in Kelvin.*

9- The configuron Gibbs free energy of ethylbenzene, $Pd_{77.5}Cu_6Si_{16.5}$, and SiO_2 as a function of temperature

This chapter is devoted to the Gibbs free energies of configurons and Phase 3 without using VFT laws. Configurons, which result from bond breaking processes and can be revealed via the minima of X-ray pair distribution functions [38], agglomerate in macroscopic percolating clusters at T_g. The coherence length in the configuron model is given in (41) [**34-36**]**:**

$$\xi(T) = \xi_0/(f(T) - f_c)^{\nu}, \quad (41)$$

where $f(T) = \frac{\exp\left(\frac{-G_d}{RT}\right)}{\left[1+\exp\left(\frac{-G_d}{RT}\right)\right]}$. (42)

The ground state corresponding to unbroken bonds and the excited state corresponding to broken bonds are separated by an energy interval G_d which is deduced from (41) and (42):

$$exp\left(\frac{-G_d}{RT}\right) = \frac{\mathrm{f(T)}}{[1-f(T)]}\ , \quad (43)$$

where $$f(T) = (1 + f_c - \frac{T_c}{T}) \quad (44)$$

is assumed to be followed by Phase 3 from T_c to T_{n+} the melting temperature of medium-range order.

G_d is the Gibbs free energy of one configuron mole when f_c = 0.15 ± 0.01 = f(T_g) is the critical threshold at T_g. Consequently, G_d (J/mole) is expected to be equal to (45) at T_c if this critical threshold value is respected:

$$G_d = 1.7346RT_g = (14.42 \pm 1) \times T_c \quad . \quad (45)$$

Equations (46) and (47) determines the value of x_3 and x_g depending on equilibrium enthalpies of the glass at T_g and of Phase 3 at T_3:

$$\Delta\varepsilon_{lg0}H_m = x_3 \times 14.42 \times T_3\ , \quad (46)$$

$$\frac{\Delta\varepsilon_{lg0}}{2}H_m = x_g \times 14.42 \times T_g\ , \quad (47)$$

where x_3 and x_g are the fractions of G_d associated with glass-forming melts and H_m is the melting heat per molecule mole. The atom number N per molecule is given in Table 3. The fraction of configuron mole per g-atom is much weaker and equal to x_3/N or to x_g/N.
The phase 3 enthalpy H_3 formed from a fragile liquid is known and equal to ($-\Delta\varepsilon_{lg0}/2\times H_m$) at T_g, ($-\Delta\varepsilon_{lg0}\times H_m$) at T_3 and ($+\Delta\varepsilon_{lg0}\times H_m$) at T_m. The Phase 3 entropy being equal to the difference S_1-S_2 is equal to zero at T_m and its Gibbs free energy equal to its enthalpy $\Delta\varepsilon_{lg0}\times H_m$. The configuron entropy is assumed to be equal to zero below the critical temperature. The Gibbs free energy $(H_3\text{-}TS_3)_c$ of Phase 3 adapted to that of configurons is represented in Figure 12 along Line 2 from T_3 = 104.66 K to T_{n+} = 202.74 K for ethylbenzene starting from an entropy (25.796 J/K/mole $+S_3$) = 0 and $H_3 = -0.17855\times H_m$ = -1637.3 J/mole at T_3. The Gibbs free energy at T_m is now equal to -2957 J/mole.

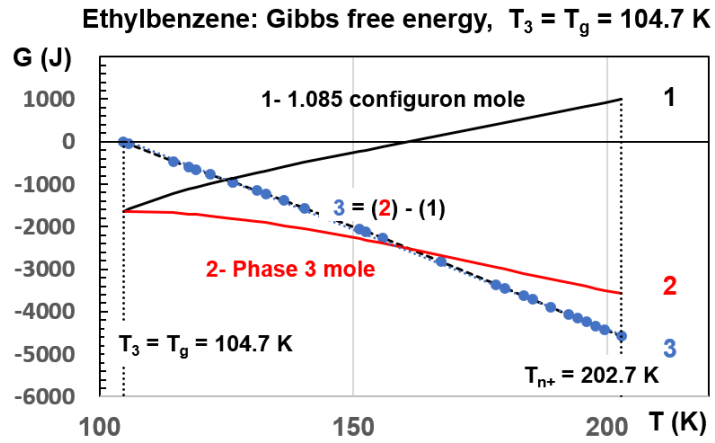

Figure 12. *Ethylbenzene: Gibbs free energies of Phase 3 in J/mole and configurons versus T (K). 1- The configuron contribution with a constant fraction $x_3 = 1.085$. 2- Contribution of configurons to Phase 3 Gibbs free energy. 3- The configuron contribution increase with temperature equal to the difference between (2) and (1).*

The configuron Gibbs free energy G_d represented along Line 1 in Figure 12 is calculated assuming that (44) is respected from T_c to T_{n+} without change of f(T) = 0.15 and then the Gibbs free energy G_d given in (43) for all glasses is only depending on T_c through (45). G_d is equal to (-1509) J per configuron mole in (45) at T_3 = 104.66 K. In these conditions, G_d is equal to (-1637.3) J/mole in Figure 12 after applying (46) with x_3 = 1.0848.

The difference between Line 2 and Line is represented by Line 3 obeying $46.7(T_3 - T)$ in perfect agreement with a thermal dependence of $\Delta e_3 = -46.3T$ (i = 11.1 using (39)) associated with atom delocalization above T_g with the freedom degree number i constant up to T_{n+}.

The same analysis is applied at T_g = 114.5 K in Figure 13 for ethylbenzene. The Gibbs free energy $(H_3\text{-}TS_3)_c$ of Phase 3 adapted to configurons is represented in Figure 13 along Line 2 from T_g = 114.5 K to T_{n+} = 202.74 K starting from an entropy (18.311 J/K/mole $+S_3$) = 0 and $H_3 = -0.08928 \times H_m$ = (-818.7) J/mole at T_g. The effective value of G_d is now 818.7 J/mole applying (47) with x_g = 0.4958. The Gibbs free energy at T_m is equal to -1624 J/mole. The difference between Line 2 and Line 1 is still represented by Line 3 obeying $27(T_g\text{-}T)$ and $\Delta e_3 = -27T$ in good agreement with the prediction of VFT laws developed in the previous chapter.

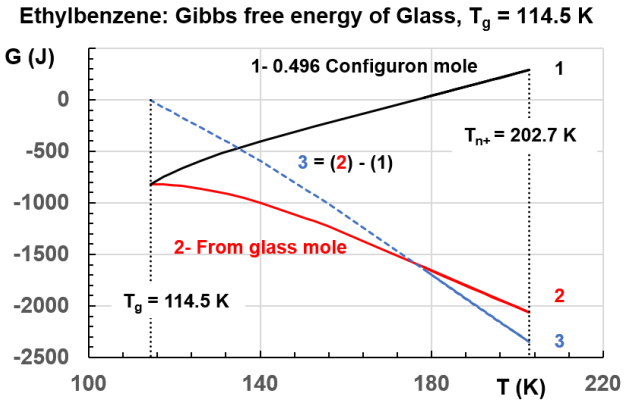

Figure 13. *Ethylbenzene: Gibbs free energies of Glass phase in J/mole and configurons versus T (K). 1- The configuron contribution with a constant fraction $x_g = 0.496$. 2- Contribution of configurons to Glass Gibbs free energy. 3- The configuron contribution increase with temperature equal to the difference between (2) and (1).*

The Gibbs free energy $(H_3\text{-}TS_3)_c$ per mole of $Pd_{77.5}Cu_6Si_{16.5}$ adapted to configurons is represented in Figure 14 along Line 2 from T_3 = 572.2 K to T_{n+} = 1218.3 K starting from an entropy (4.7328 J/K/mole $+S_3$) = 0 and $H_3 = -0.19839 \times H_m$ = -1696.1 J/mole at T_3. The Gibbs free energy at T_m is now equal to -3302 J/mole. The Gibbs free energy G_d is equal to 8251.7 J per configuron mole at T_3 = 572.2 K. In this liquid alloy, the effective Gd is equal to 1696.1 J/mole multiplying 8251 by x_3 = 0.2055 in Figure 14. The difference between Line 2 and Line 1 is represented by Line 3 obeying 8.39 (T_3-T) and Δe_3 = -8.39T (i = 2.02 using (39)).

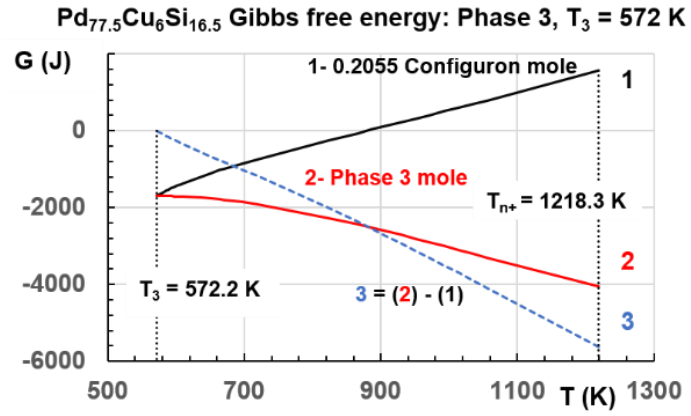

Figure 14. *$Pd_{77.5}Cu_6Si_{16.5}$: Gibbs free energies of phase 3 in J/mole and configurons versus T (K). 1- The configuron contribution with a constant fraction x_3 = 0.2055. 2- Contribution of configurons to Phase 3 Gibbs free energy. 3- The configuron contribution increase with temperature equal to the difference between (2) and (1).*

The phase 3 enthalpy H_3 formed from a strong liquid is equal to $(-\Delta\varepsilon_{lg0} \times H_m)$ at T_g, $(-\Delta\varepsilon_{lg0} \times H_m)$ at T_3 and $(+\Delta\varepsilon_{lg0} \times H_m)$ at T_m. The Gibbs free energy $G_3 = (H_3\text{-}TS_3)$ of SiO_2 Phase 3 adapted to configurons is represented in Figure 15 along Line 2 from T_3 = 1256.36 K. The Phase 3 entropy at T_m being equal to the difference $S_1\text{-}S_2$ is equal to zero and its Gibbs free energy equal to its enthalpy $\Delta\varepsilon_{lg0} \times H_m$. G_3 per mole of SiO_2 is represented in Figure 15 along Line 2 from T_3 = 1256.36 K to T_{n+} = 2154.6 K starting from $(1.062+S_3) = 0$ and $H_3 = -0.08754 \times H_m$ = -787.9 J/mole at T_3. The Gibbs free energy at T_m is now equal to -1331.9 J/mole. The Gibbs free energy G_d is equal to 18117 J per configuron mole at T_3 = 1256.36 K. In this liquid alloy, the effective G_d is equal to -787.9 J/mole multiplying 18117 by x_3 = 0.04348 in Figure 15. The difference between Line 2 and Line 1 is represented by Line 3 obeying 1.88 (T_3-T) and Δe_3 = -1.88T (i = 0.45 using (39)).

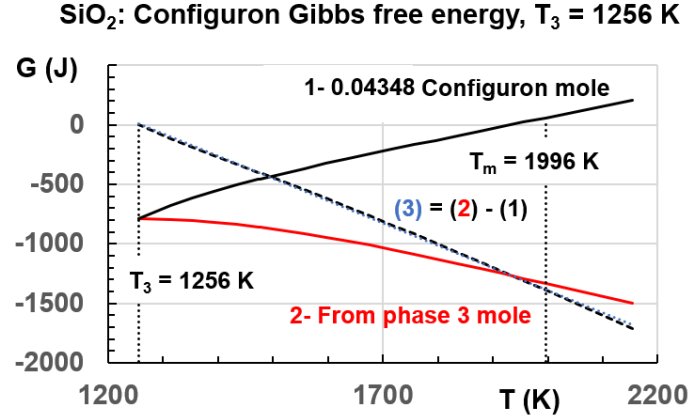

Figure 15. *SiO_2: Gibbs free energies of Phase 3 in J/mole and configurons versus T (K). 1- The configuron contribution with a constant fraction x_3 = 0.04348. 2- Contribution of configurons to Phase*

3 Gibbs free energy. 3- The configuron contribution increase with temperature equal to the difference between (2) and (1).

The Gibbs free energy $G(H_3\text{-}TS_3)_c$ per mole of SiO_2 adapted to configurons is represented in Figure 16 along Line 2 from T_g = 1473 K to T_{n+} = 2154.6 K starting from an entropy $(0.48084+S_3) = 0$ and an enthalpy equal to zero at T_g. The Gibbs free energy at T_m is now equal to -171.9 J/mole. The Gibbs free energy G_d is equal to (-21243) J per configuron mole at T_g = 1473 K. The effective G_d is equal to -787.9 J/mole multiplying 21243 by x_g = 0.037086 in Figure 16. The difference between Line 2 and Line 1 with adding +787.9 J is represented by Line 3 obeying $1.376(T_g\text{-}T)$ and Δe_3 = -1.376 T (i = 0.33 with (39)) while the VFT model leads to Δe_3 = 2.06 T.

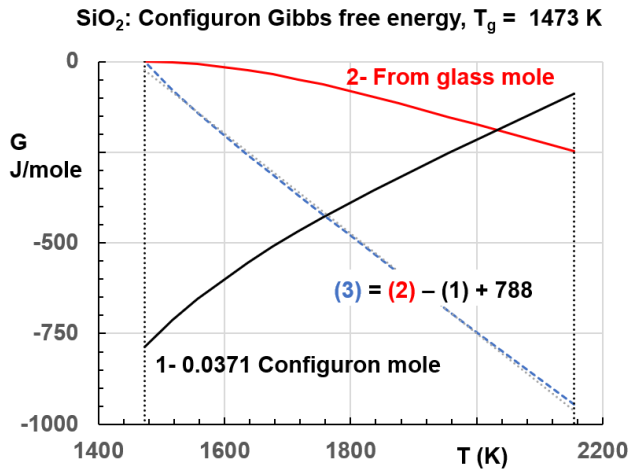

Figure 16. *SiO_2: Gibbs free energies of Glass phase and configurons versus T (K). 1- The configuron contribution with a constant fraction x_g = 0.0371. 2- Contribution of configurons to Glass Gibbs free energy with an endothermal latent heat $\Delta\varepsilon_{lg0}\times H_m$ at T_g. 3- The configuron contribution increase with temperature equal to the difference between (2) and (1) after transition.*

The number i characterizing the entities moving into the melt from T_g up to T_{n+} is small and still much smaller for strong than for fragile liquids. It does not depend on temperature due to the medium-range order of Phase 3. The fraction of volume being ordered is constant and equal to $f_c = 0.15 \pm 0.01$. The configuron Gibbs free energy G_d (T) starting from T_3 with zero entropy in strong liquids is viewed as having an equilibrium enthalpy equal to $-\Delta\varepsilon_{lg0}\times H_m$. It cannot start from T_g with an entropy and an enthalpy equal to 0 and consequently a latent heat at T_g is needed to explain the formation of configurons. This latent heat also exists at equilibrium in fragile liquids, G_d(T) starting with a zero entropy at T_3 and an equilibrium enthalpy equal to $-\Delta\varepsilon_{lg0}\times H_m$ up to T_g. This case is not considered but even it would lead to a latent heat equal to $\Delta\varepsilon_{lg0}\times H_m$. This analysis still show that the supplementary configuron number induced above T_c is proportional to $(T_c - T)$ in agreement with predictions of Sanditov et al [42] and with the configuron model. A frozen enthalpy equal to the equilibrium enthalpy $-\Delta\varepsilon_{lg0}\times H_m$ of Phase 3 and of glasses is needed up to T_g to explain the negative value of G_d at T_c [34-36]. The Phase 3 formation and configuron models are inseparable.

The main conclusion of this chapter is that the volume fraction of Phase 3 being "ordered" from T_3 up to T_{n+} involve 15% of all atoms building the 'ordered' melt. The delocalization energy evaluation comparing the Gibbs free energies of Phase 3 and configurons leads to the same value for a fragile liquid than that obtained from VFT laws. The agreement between the two models is not as good for a strong liquid. The two models developped here predict that the atom delocalization energy is proportional to the temperature in agreement with predictions of Sanditov et al [42].

10- Gibbs free energy of configurons in 54 glasses at T_3

The phase 3 enthalpies of 54 melts equal to $-\Delta\varepsilon_{lg0}H_m$ below T_3 are those of configurons. The fraction x_3 has to be multiplied by the configuron Gibbs free energy G_d at T_3 to obtain $-\Delta\varepsilon_{lg0}H_m$. The values of x_3 and x_3/N are given in Table 5 where N is the atom number of each molecule. The melting heat H_m in

kJ/mole, the enthalpy coefficient $\Delta\varepsilon_{lg0}$, the Gibbs free energy $\Delta\varepsilon_{lg0}H_m/N$ in J/g.atom equal to G_dx_3/N and the Gibbs free energy G_d in Joules per configuron mole calculated with (45) are given in Table 5.

Table 5. Materials data used in and resulting from calculations

	Materials	N	H_m	x_3	x_3/N	$\Delta\varepsilon_{lg0}$	$\Delta\varepsilon_{lg0}*H_m/N$	G_d	G_dx_3/N
1	b-D-Fructose	24	32	1.01	0.0420	0.12169	164	3919	164
2	Probucol	83	36	1.16	0.0139	0.13033	56	4022	56
3	Griseofulvin	41	38	1.00	0.0243	0.13083	120	4961	120
4	D-glucose	24	32	1.02	0.0424	0.13214	178	4208	178
5	1,3,5-tri-α-Naphtylbenzene	60	33	1.03	0.0171	0.14211	79	4602	79
6	Phenobarbital	29	28	0.93	0.0319	0.14318	138	4314	138
7	Isopropyl benzene	21	7	0.64	0.0304	0.14689	51	1686	51
8	Hydro-chloro-thiazide	25	34	0.96	0.0383	0.14808	199	5190	199
9	3-Methylpentane	20	5	0.77	0.0384	0.15000	40	1037	40
10	m-Cresol	16	11	0.60	0.0376	0.15210	100	2676	100
11	Xylitol	22	34	1.66	0.0754	0.15922	246	3264	246
12	Phenolphthalein	38	47	1.55	0.0407	0.15947	198	4855	198
13	9-Bromophenanthrene	34	15	0.79	0.0233	0.16012	70	3008	70
14	a-Phenil -cresol	26	23	1.31	0.0503	0.16463	148	2931	148
15	H2SO4-3H2O	16	24.22	1.92	0.1200	0.16667	252	2102	252
16	Diethylphthalate	30	17.99	1.27	0.0422	0.16667	100	2368	100
17	m-Fluorotoluene	15	8.3	0.84	0.0560	0.16576	92	1638	92
18	2-methyl tetrahydrofuran	16	6.65	0.92	0.0577	0.16788	70	1210	70
19	n-Butene	16	3.96	0.88	0.0548	0.17045	42	769	42
20	Toluene	12	6.64	0.73	0.0611	0.17135	95	1551	95
21	Glycerol	15	18.3	1.27	0.0848	0.17466	213	2512	213
22	2-Methylpenthane	14	6.26	1.06	0.0759	0.17500	78	1031	78
23	Ethylbenzene	20	9.17	1.08	0.0542	0.17855	82	1509	82
24	n-Propanol	18	5.4	0.77	0.0427	0.18000	54	1264	54
25	3-Bromopenthane	11	8.4	1.10	0.1001	0.18263	139	1392	139
26	$CaAl_2Si_2O_8$	17	135.6	1.63	0.0959	0.18306	1460	15233	1460
27	2-methyl-1-propanol	23	6.32	0.85	0.0371	0.18895	52	1398	52
28	Selenium	15	5	0.23	0.0155	0.18851	63	4043	63
29	$CaMgSi_2O_6$	10	138.1	2.10	0.2102	0.19820	2737	13020	2737
30	Butyronitrile	10	5.02	0.79	0.0794	0.19876	100	1256	100
31	cis-/trans-Decalin	12	9.46	1.09	0.0908	0.20346	160	1766	160
32	Ethanol	18	4.98	0.85	0.0472	0.20625	57	1208	57

33	Methanol	9	3.85	0.63	0.0699	0.20930	90	1281	90
34	Ethylene glycol	6	11.86	1.28	0.2142	0.20962	414	1934	414
35	m-Xylene	10	11.56	1.59	0.1593	0.22000	254	1596	254
	BMG								
36	$Pd_{40}Ni_{10}Cu_{30}P_{20}$	1	6.82	0.12	0.1199	0.13784	940	7844	940
37	$Pd_{43}Ni_{10}Cu_{27}P_{20}$	1	7.01	0.13	0.1266	0.14090	988	7802	988
38	$Au_{49}Ag_{5.5}Pd_{2.3}Cu_{26.9}Si_{16.3}$	1	5.1	0.16	0.1624	0.17008	867	5341	867
39	$Pd_{40}Ni_{40}P_{20}$	1	9.4	0.21	0.2080	0.17131	1610	7719	1610
40	$Pt_{57.3}Cu_{14.6}Ni_{5.3}P_{22.8}$	1	11.4	0.33	0.3252	0.19261	2196	6646	2196
41	$Zr_{46}Cu_{46}A_{l8}$	1	8.04	0.17	0.1663	0.19595	1575	9311	1575
42	$Zr_{58.5}Cu_{15.6}Ni_{12.8}Al_{10.3}Nb_{2.8}$	1	8.7	0.19	0.1945	0.19839	1726	8763	1726
43	$Pd_{77.5}Cu_{6}Si_{16.5}$	1	8.55	0.21	0.2055	0.19904	1702	8251	1702
44	$Zr_{45}Cu39.3Al7Ag8.7$	1	7.93	0.18	0.1764	0.20168	1599	8945	1599
45	$Cu47Ti_{34}Zr_{11}Ni_{8}$	1	11.3	0.26	0.2623	0.21042	2378	8690	2378
46	$Mg_{65}Cu_{25}Y_{10}$	1	8.65	0.33	0.3322	0.21310	1843	5478	1843
47	$Zr_{65}Cu_{17.5}Ni_{10}Al_{7.5}$	1	10.3	0.26	0.2618	0.21655	2230	8385	2230
48	$La_{55}Al_{25}Ni_{5}Cu_{10}Co_{5}$	1	6.08	0.22	0.2221	0.21780	1324	5926	1324
49	$Zr_{65}Cu_{27.5}\ Al_{7.5}$	1	12.8	0.33	0.3296	0.22036	2821	8457	2821
50	$La_{55}Al_{25}Ni_{10}Cu_{10}$	1	6.82	0.25	0.2542	0.23778	1622	5913	1622

The values of x_3 are plotted in Figure 17 as a function of their number in Table 5 varying from zero to 50; the numbers 51 to 54 are those of SiO_2, GeO_2, N-butanol and BeF_2. There is one configuron mole per mole of Phase 3 for $x_3 = 1$. This is true for many glasses in agreement with the configuron model [34-36]. The values x_3 are much smaller for all BMG even for selenium N°28. The Gibbs free energy of BMG configurons is much smaller than those of insulating molecular glasses. Short-range order tends to reduce the configuron contribution and the melting heat by a fraction recovered at higher temperatures than T_m. The broken bond fraction x_3 is enhanced above 1 in several molecular glasses.

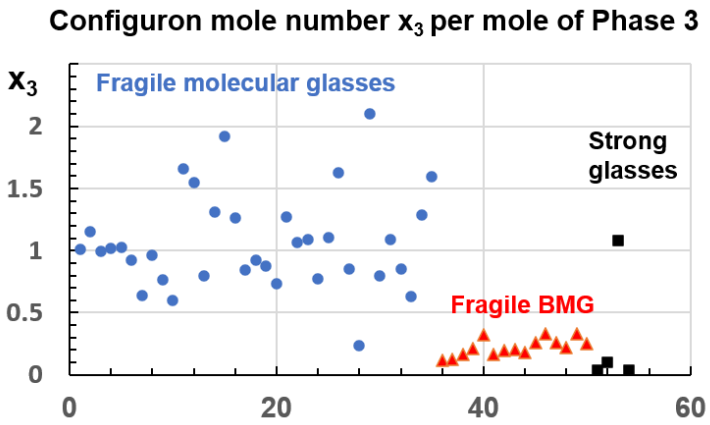

Figure 17. *Configuron mole number x_3 at the formation temperature T_3 of Phase 3 versus the number in column 1 of Table 5 and vs 51 to 54 for SiO_2, GeO_2, N-butanol and BeF_2.*

11- Melt memories

Glass and configuron phases are described by their enthalpy and entropy at equilibrium. They give rise to memory effects up to a temperature $T_{n+} > T_m$ through medium-range order. Enthalpy relaxation is measured after hours or days and even 1.5 year of isothermal aging in various glasses [127-133]. All these results imply that enthalpy recovery exhibits two times scales of equilibrium in agreement with two activation energies as shown in chapter 7-3. Other high enthalpy reductions are still observed below T_{g1} after vapor deposition with glass transition temperatures increasing from T_{g1} to $T_{g2} \cong 1.1T_{g1}$ and even up to $T_{g3} \cong 1.2\ T_{g1}$. Thermodynamic properties of isothermally annealed and vapor-deposited glasses characterized by a heat capacity jump equal to $1.5S_m$ at T_g are successively analyzed. In all examples, the authors have considered, up to now, that all melts reproduce the enthalpy and the specific heat of the initial liquid and consequently they consider that these melts have no memory of the glass phase transition giving rise to the melt. Our model predicts that the glass phase characterizes and determines the thermodynamic properties of the melt. The following experimental results agree with this assumption.

11-1 Enthalpy recovery of polystyrene PS85k after isothermal aging below T_{g1}.

The specific heat of this polymer is obtained by D.C. Cangialosi et al using DSC measurements after aging at T = 363 K and represented in Figure 18. Its maximum duration attains 322 days. Its initial glass transition temperature before aging is T_{g1} = 379.5 K and the specific heat difference between melt and glass is 0.3075 J/K/g [128]. The melting entropy is $S_m = \Delta C_p / 1.5 = 0.205$ J/K/g. The melting temperature T_m is assumed to be 548 K [134] and the melting enthalpy H_m = 112.34 J/g. The enthalpy coefficients of liquids 1, 2 and 3 are given in (48-50) applying (3-8) for a = 1 and T_{g1} = 379.5 K:

$$\varepsilon_{ls} = 1.69252(1 - 4.3234 \times \theta^2)\ , \qquad (48)$$

$$\varepsilon_{gs} = 1.53878(1 - 3.1703 \times \theta^2), \qquad (49)$$

$$\Delta\varepsilon_{lg} = 0.15374 - 2.439 \times \theta^2\ . \qquad (50)$$

The recovered enthalpy after 322 days of aging is 3.2 J/g/K [127]; the corresponding enthalpy coefficient is $3.2/H_m = 0.0284$. The glass transition temperature after aging is predicted equal to T_{g2} = 389.9 K with (3) and an increase of ε_{gs0} equal to 0.0284. The recovered enthalpy is evaluated from the difference between the specific heat shown in Figure 18 and that of the same sample quenched after aging from T_g + 30 K down to 363 K, the quenched sample having the specific heat of the glass with T_{g2} = 389.9 K instead of T_{g1} = 379.5 K. Consequently, there is a constant difference of enthalpy between the two glass phases which does not contribute to the specific heat.

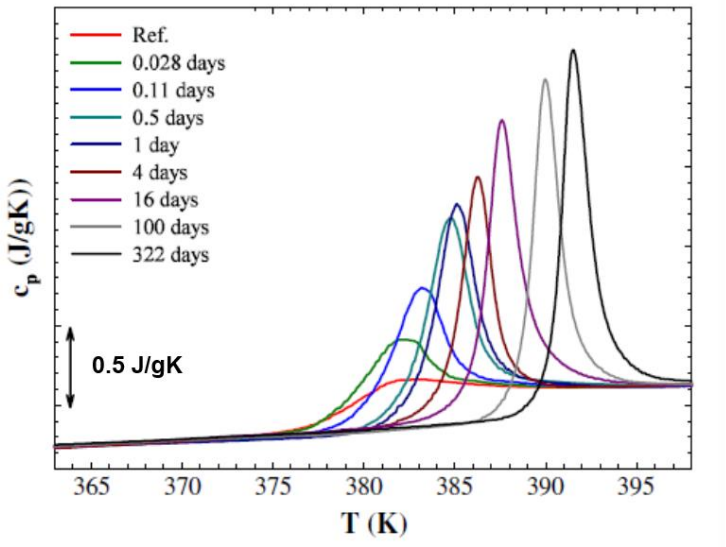

Figure 18: *Reproduced from [127] [D. Cangiolasi, V.M. Boucher, A. Alegria, and J. Colmenero, Phys. Rev. Lett. 111 (2013) 095701] with permission of APS. The C_p scale is equal to 0.5 J/g/K with the agreement of authors. Specific heat versus temperature as obtained by DSC for Polystyrene 85k at different aging times.*

The enthalpy coefficients of the aged sample with T_{g2} = 389.9 K are given in (51-53):

$$\varepsilon_{ls} = 1.7115(1 - 4.5568 \times \theta^2) \ , \tag{51}$$

$$\varepsilon_{gs} = 1.56724(1 - 3.3174 \times \theta^2) \ , \tag{52}$$

$$\Delta\varepsilon_{lg} = 0.14425 - 2.5998 \times \theta^2) \ . \tag{53}$$

The enthalpy coefficients $\Delta\varepsilon_{lg}$ of configurons before and after aging are represented in Figure 19. After aging, the temperature T_{n+} and the enthalpy are weakened at high temperature.

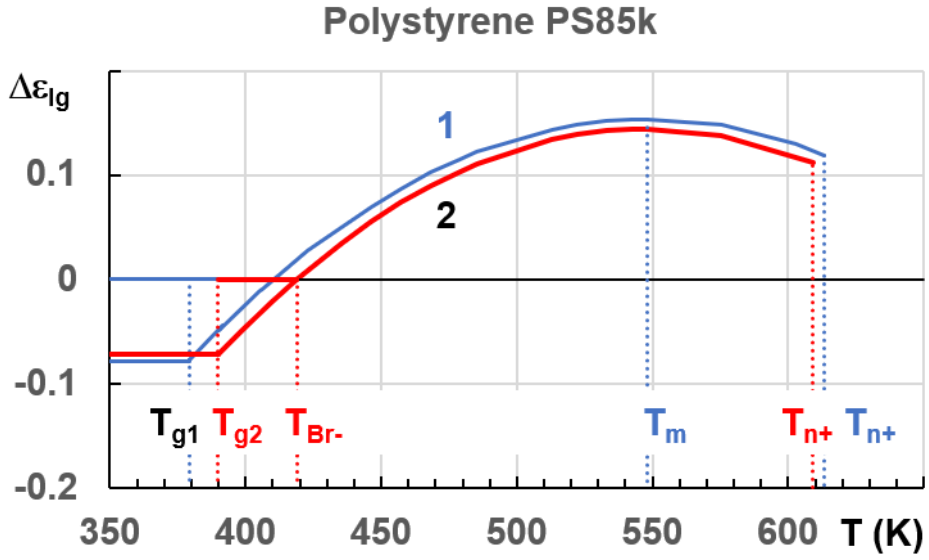

Figure 19: *The enthalpy coefficients $\Delta\varepsilon_{lg}$ of Phase 3 represented on blue Line 1 before aging and on red Line 2 after aging. T_{g1} = 379.5 K, T_{g2} = 389.9 K, T_{Br-} = 418.9 K, T_m = 548 K, T_{n+} = 609.2 and 613.3 K.*

11-2 **Formation of stable phases by vapor deposition with $T_{g2} \cong 1.1\ T_{g1}$**

Many new phases with reduced enthalpy have been discovered by vapor deposition below T_{g1}. The glass transition temperatures T_{g2} of these thin films are higher than those of bulk materials [135-146]. Cooling these films from above T_{g2} does not lead to a glass transition at T_{g1}. The transition after new cooling and reheating leads to a transition at T_{g2} instead of T_{g1} in contradiction with all expectations and author conclusions. All these melts are transformed at the new glass transition temperatures T_{g2}. Melt enthalpy is changed by the increase of T_g. In Figure 20, the specific heat of ethylene glycol is reproduced as an example among many other vapor-deposited materials with T_{g2} = 167 K, $T_{g1} \cong$ 150 K and T_m = 260.5 K [136,147].

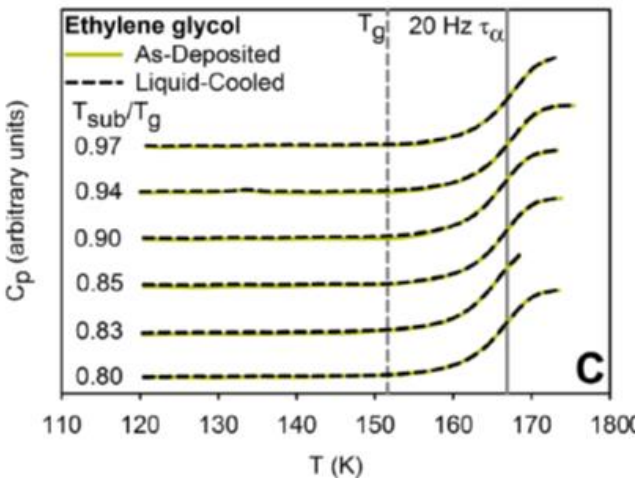

Figure 20: *Temperature ramping AC nanocalorimetry experiments of ethylene glycol glass. Reproduced from [136] [M. Tylinski, Y.Z. Chua, M.S. Beasley, C. Schick, and M.D. Ediger, J. Chem. Phys. 145 (2016) 174306] with permission of AIP Publishing. The solid colored lines are as-deposited glass while the dashed black curves are liquid-cooled glasses. The curves for different substrates temperatures have been shifted. The noted value of T_g is the temperature when τ_α =100 s.*

The enthalpy coefficients of liquids 1, 2 and 3 in ethylene glycol are given in (54-59) applying (3-8) for a = 1, T_{g1} = 150 K and T_{g2} = 167 K:

For T_{g1} = 150 K,

$$\varepsilon_{ls} = 1.57582(1 - 3.3661 \times \theta^2) \ , \tag{54}$$

$$\varepsilon_{gs} = 1.36372(1 - 2.593 \times \theta^2) \ , \tag{55}$$

$$\Delta\varepsilon_{lg} = 0.21209 - 1.7682 \times \theta^2) \ . \tag{56}$$

For T_{g2} = 167 K,

$$\varepsilon_{ls} = 1.64107(1 - 3.8199 \times \theta^2) \ , \tag{57}$$

$$\varepsilon_{gs} = 1.46161(1 - 2.859 \times \theta^2) \ , \tag{58}$$

$$\Delta\varepsilon_{lg} = 0.17946 - 2.0904 \times \theta^2) \ . \tag{59}$$

The enthalpy coefficients $\Delta\varepsilon_{lg}$ of configurons before and after aging are represented in Figure 21. After vapor deposition, the temperature T_{n+} and the enthalpy are weakened above T_{g2}. The enthalpy coefficient of a lot of vapor-deposited films is nearly equal to $\Delta\varepsilon_{lg0}/2$. In fact, it is equal to the $\Delta\varepsilon_{lg0}/2$ of the deposited glass at T_{g2} as shown in Figure 21.

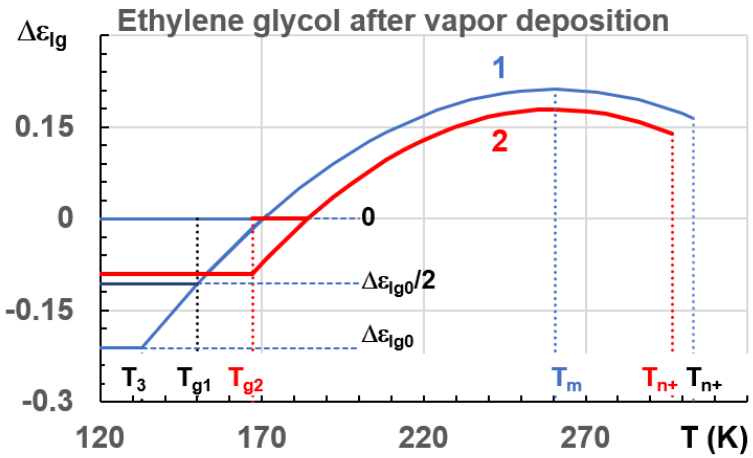

Figure 21: *The enthalpy coefficients $\Delta\varepsilon_{lg}$ of Phase 3 represented on blue Line 1 for a bulk material and on red Line 2 after vapor deposition. Temperatures T_3 = 132.9 K, T_{g1} = 150 K, T_{g2} = 167 K, T_m = 260.5 K, T_{n+} = 296.7 and 303.3 K. The enthalpy coefficients of three glass phases are zero, $-\Delta\varepsilon_{lg0}/2$ and $-\Delta\varepsilon_{lg0}$. The third one is not obtained.*

11-3 **Formation of stable phases by vapor deposition with $T_{g3} \cong 1.2T_{g1}$**

Highest enthalpy variations and higher values of T_{g3}/T_{g1} are observed using growth rates spanning 0.001 to 0.1 nm/s for vapor deposition [148,149]. The glass enthalpy is now equal to the enthalpy ($-\Delta\varepsilon_{lg0}$) of Phase 3. The specific heat of ethylbenzene deposited glass is represented as a function of temperature in Figure 22 and measured during first and second heating separated by slow cooling from temperature higher than T_m = 178.1 K. The melt enthalpy is changed after a glass transition temperature increase from T_{g1}= 114.5 K [18,91] to T_{g3} = 135.7 K. (T_{g3}) is calculated from (1) with $\Delta\varepsilon$ = 0.17855, ε_{gs0} = 1.6429 and θ_{0g}^2 = 0.34862 as given by (3,4).

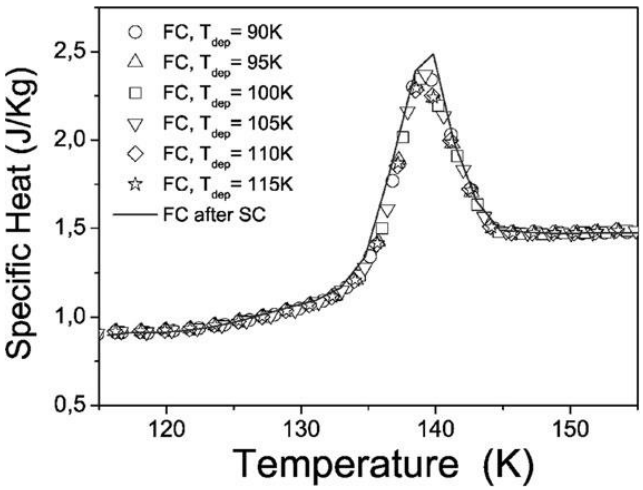

Figure 22. ***Melting temperature of Phase 3 after stabilization by vapor deposition of ethylbenzene films.*** *Reproduced from [148] [E. Leon-Gutierrez, A. Sepulveda, G. Garcia, M.T. Clavaguera-Mora, and J. Rodriguez-Viejo, Phys. Chem. Chem. Phys.12 (2010) 14693-14698] with the permission of Royal Society of Chemistry. Second and subsequent calorimetric upscans (Fast-Cooled samples and FC after SC Slow-Cooling) from vapor deposited samples at different temperatures. Transition temperature at T_{g3} = 135.7 K instead of T_g = 114.5 K for the bulk glass phase.*

The enthalpy coefficients of liquids 1, 2 and 3 in ethylbenzene are given in (60-65) applying (3-8) for a = 1, T_{g1} = 114.5 K and T_{g3} = 135.7 K:

T_{g1} =114.5 K,

$$\varepsilon_{ls} = 1.6429 \times (1 - \theta^2/0.26075), \quad (60)$$

$$\varepsilon_{gs} = 1.46435 \times (1 - \theta^2/0.34861), \quad (61)$$

$$\Delta\varepsilon_{ls} = 0.17855 - 2.1002 \times \theta^2. \quad (62)$$

T_{g3} = 135.7 K,

$$\varepsilon_{ls} = 1.7619 \times (1 - \theta^2 \times 5.3634), \quad (63)$$

$$\varepsilon_{gs} = 1.64285 \times (1 - \theta^2 \times 3.8346), \quad (64)$$

$$\Delta\varepsilon_{ls} = 0.11905 + 0.11905/2 - 3.15 \times \theta^2. \quad (65)$$

The quantity 0.11905/2 is added in (65) to obtain a glass transition with $\Delta\varepsilon_{lg}$ = 0 at T = T_{g3} and an enthalpy change equal to $\Delta\varepsilon_{lg0} \times H_m$ in agreement with Figure 22. The glass transition temperature T_{g3} is predicted using (1) and $\Delta\varepsilon = \Delta\varepsilon_{lg0}$ = 0.17855 given in (62). The enthalpy coefficients $\Delta\varepsilon_{lg}$ in (62,65) are represented in Figure 23. After vapor deposition, the temperature T_{n+} and the enthalpy above T_{g3} are weakened.

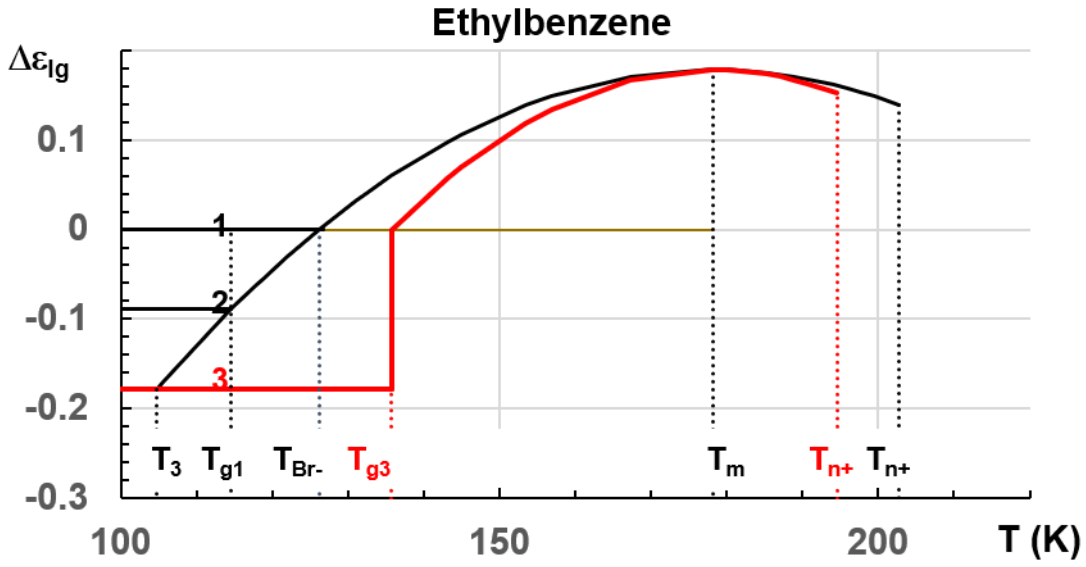

Figure 23: *The enthalpy coefficients $\Delta\varepsilon_{lg}$ of configurons represented in black (upper line) for a bulk material and in red (lower line) after vapor deposition. Temperatures T_3 = 104.7 K, T_{g1} = 114.5 K, T_{g3} = 135.7 K, T_m = 178.1 K, T_{n+} = 200.8 and 202.7 K. The enthalpy coefficients of three glass phases 1, 2 and 3 are zero, $-\Delta\varepsilon_{lg0}/2$ and $-\Delta\varepsilon_{lg0}$. The third one is obtained by vapor deposition [148] as shown in Figure 22.*

Conclusions:

A new description of glasses is proposed as being intermediate phases masking the initial formation of a supercooled thermodynamic phase which can be superheated. A two-liquid model is

applied, after quenching a melt from high temperatures to a frozen amorphous state, without undergoing any phase transition during the rapid cooling. A subsequent annealing always induces an enthalpy recovery leading to the equilibrium of a new thermodynamic phase called Phase 3 and to that of the glass phase, followed by the glass transition at T_g. The Gibbs free energy of Phase 3 is equal to the difference of Gibbs free energy G_3 of two liquids. Phase 3 is a new liquid characterized by a medium-range order which can be superheated up to a temperature T_{n+} higher than T_m where this order disappears accompanied by latent heat. The temperatures T_3 and T_{n+} and the enthalpies changes at these temperatures are predicted for 54 glasses. The existence of this new phase has been searched, thirty years ago, with the power law coming from the dynamic scaling theory which is successfully applied to the phase transition of spin glasses.

An 'ordered' phase 3 now cooled from a temperature weaker than T_{n+} undergoes a glass transition at T_g without attaining the equilibrium enthalpies of glass and Phase 3. The glass phase masks the existence of Phase 3 as shown in other chemical transformations. The activation energy of Phase 3 is negative between T_3 and T_g. The glass transition occurs in many glasses at a temperature where this activation energy is equal to zero. These properties confirm the phase 3 existence behind the glass phase.

The Phase 3 properties are successfully analyzed in the light of configuron percolation theory with a percolation threshold $\Phi = 0.15 \pm 0.01$. The Gibbs free energy $x_3 \times G_d$ of configurons at the critical temperature T_c is determined from the Gibbs free energy G_3 J/mole of Phase 3 from the assumption that the kinetic 'ordered' entities of Phase 3 involve 15% of all atoms present in the melt up to T_{n+}. The coefficient x_3 is chosen to equalize $x_3 \times G_d$ with the equilibrium enthalpies of Phase 3 and glass just below the critical temperature T_c. The coefficient x_3 is equal to 1 for many molecular glasses in quantitative agreement with the theoretical value of G_d J/g-atom. This coefficient is much smaller for all metallic glasses. Other molecular glasses have weaker and higher x_3 than one. Another consequence from model proposed is that the glass phase characterizes and determines the thermodynamic properties of the melt.

The enthalpy at T_{n+} is reduced toward the equilibrium enthalpy of the liquid without mean-range order for which $\Delta\varepsilon_{lg} = 0$. The average value of the enthalpy coefficient variation $\Delta\varepsilon_{lg}$ at T_{n+} of 50 fragile liquids is 0.13746 and corresponds to a volume fraction of ordered phase given by the critical threshold equal to 0.15 ± 0.01. The corresponding average for SiO_2, GeO_2 and BeF_2 is 0.0728.

The size of specific heat jump at T_g is discussed and the heating rate dependence of the glass transition is accompanied by weak latent heats. The relaxation times above T_g from fragile Liquid 1 to fragile Liquid 2 of $Au_{49}Ag_{5.5}Pd_{2.3}Cu_{26.9}Si_{13.3}$ and $Zr_{65}Cu_{27.5}$ $Al_{7.5}$ are predicted in agreement with experiments. The glass transition temperature is lowered when the sample is stored after liquid quenching at a temperature higher than the lowest nucleation temperature in liquid 2 or submitted to long aging before attaining T_g with the first slow heating. The first-order transition, recently observed, towards a quasi-crystalline phase of $Mg_{69}Zn_{27}Yb_4$ is quantitatively predicted at the right temperature with the same equations than those used to explain the formation of glacial phases in water, d-mannitol, triphenyl phosphite, and n-butanol.

Références

1. **H. Tanaka.** Two-order parameter model of the liquid-glass transition. I. Relation of the liquid-glass transition and crystallization. *J. Non-Cryst. Sol.* 351 (2005) 3371-3384.

2. **A. V. Evteev, A. T. Kosilov, E. V. Levchenko, O. B. Logachev.** Kinetics of isothermal nucleation in a supercooled iron melt. *Phys. Sol. State.* 48 2006) 577-582.

3. **P. J. Steinhard, D. R. Nelson, M. Ronchetti.** Bond-orientational order in liquid and glasses. *Phys. Rev. B 28 (*1983) 784-805.

4. **E. W. Fischer, G. Meier, T. Rabenau, A. Patkowski, W. Steffen, and W Thonnes.** Density fluctuations around the glass-transition, of low molecular weight glass-forming liquids. *J. Non-Cryst. Solids, 131-133 (*1991) 134-138.

5. **A. S. Bakai.** Long-range density fluctuations in glass-forming melts. *J. Non-Cryst. Sol.* 307-310 (2002) 623-629.

6. **A. S. Kolokol and A. L. Shimkevitch.** Topological structure of liquid metals. *At. Énerg.* 98 (2005) 187-190.

7. **R.F. Tournier and E. Beaugnon.** Texturing by cooling a metallic melt in a magnetic field. *Sci. Technol. Adv. Mater.* 10 (2009) 014501.

8. **R.F. Tournier.** Crystallization of supercooled liquid elements induced by superclusters containing magic atom numbers. *Metals.* 4 (2014) 354-387.

9. **Y. He, J. Li. J. Wang, H. Kou, E. Beaugnon.** Liquid-liquid structure transition and nucleation in undercooled Co-B eutectic alloys. *Applied Physics A.* 123 (2017) 391.

10. **Y. Yue.** Experimental evidence for the existence of an ordered structure in a silicate liquid above its liquidus temperature. *J. Non-Cryst. Sol.* 345-346, (2004) 523-527.

11. **D. Turnbull.** Kinetics of solidification of supercooled liquid mercury. *J. Chem. Phys.* 20 (1952) 411.

12. **K.F. Kelton.** Crystal nucleation in liquids and glasses. *Sol. State Phys.* 45 (1991) 75-177.

13. **R.F. Tournier.** First-order transitions in glasses and melts induced by solid superclusters nucleated and melted by homogeneous nucleation instead of surface melting. *Chem. Phys.* 524 (2019) 40-54.

14. **Y. Waseda, S. Takeda.** Structural inhomogeneity in liquid alloys. *Chin. J. Phys.* 31(2) (1993) 235.

15. **C. Way, P. Wadhwa, R. Busch.** The influence of shear rate and temperature on the viscosity and fragility of the $Zr_{41.2}Ti_{13.8}Cu_{12.5}Ni_{10.0}Be_{22.5}$ metallic-glass-forming liquid. *Acta Materialia.* 55 (2007) 2977-2983.

16. **R.F. Tournier.** Homogeneous nucleation of phase transformations in supercooled water. *Physica B.* 579 (2020) 411895.

17. **S. Wei, F. Yang, J. Bednarcik, I. Kaban, O. Shuleshova, A. Meyer & R. Busch.** Liquid-liquid transition in a strong bulk metallic glass-forming liquid. *Nature Commun.* 4 (2013) 2083.

18. **K. Ishii, H. Nakayama, S. Hirabayashi, R. Moriyama.** Anomalously high-density glass of ethylbenzene prepared by vapor deposition at temperatures close to the glass-transition temperature. *Chem. Phys. Lett.* 459 (2008) 109-112.

19. **A. Inoue, T. Zhang, T. Masumoto.** The structural relaxation and glass transition of La-Al-Ni and Zr-Al-Cu amorphous alloys with a significant supercooled liquid region. *J. Non-Cryst. Sol.* 150 (1992) 396.

20. **L-M. Wang, S. Borick, C.A. Angell.** An electrospray technique for hyperquenched glass calorimetry studies: propylene glycol and di-n-butylphthalate. *J. Non-Cryst. Sol.* 353 (2007) 3829-3837.

21. **L. Hornboll, Y. Yue.** Enthalpy relaxation in hyperquenched glasses of different fragility. *J. Non-Cryst. Sol.* 354 (2008) 1832-1870.

22. **L. Hu, C. Zhang, and Y. Yue.** Thermodynamic anomaly of the sub-Tg relaxation in hyperquenched metallic glasses. *J. Chem. Phys.* 138 (2013) 174508.

23. **R. F. Tournier.** Glass phase and other multiple liquid-to-liquid transitions resulting from two-liquid competition. *Chem. Phys. Lett.* 665 (2016) 64-70.

24. **W. Kauzmann.**The nature of the glassy state and the behavior of liquids at low temperatures. *Chem. Rev.* 43(2) (1948) 219.

25. **R. F. Tournier.** Presence of intrinsic growth nuclei in overheated and undercooled liquid elements. *Physica B.* 392 (2007) 79-91.

26. **R.F. Tournier.** Fragile-to-fragile liquid transition at Tg and stable-glass phase nucleation rate maximum at the Kauzmann temperature. *Physica B,* 454 (2014) 253-271.

27. **P.H. Poole, F. Sciortino, U. Essmann, H.E. Stanley.** Phase behavior of metastable water. *Nature.* . 360 (1992) 324-328.

28. **C. Desgranges and J. Delhommelle.** Communication: Existence and control of liquid polymorphism in methanolunder shear. *J. Chem. Phys.* 149(11) (2018) 111101.

29. **C. Desgranges and J. Delhommelle**. Role of liquid polymorphism during the crystallization of silicon. *J. Am. Chem. Soc,* 133 (2011) 2872-2874.

30. **R.P. Wool.** Twinkling fractal theory of the glass transition. *J. Polymer Sci. Part B, Polym. Phys.* 46 (2008) 2765-2778.

31. **R.P. Wool, A. Campanella.** Twinkling fractal theory of the glass transition: rate dependence and time-temperature superposition. *J. Polymer Sci. Part B Polym. Phys.* 47 (2009) 2578-2589.

32. **J.F. Stanzione III, K.E. Strawhecker, R.P. Wool.** Observing the twinkling nature of the glass transition. *J. Non-cryst. Sol.* 357 (2011) 311.

33. **C.A. Angell, K.J. Rao.** Configurational excitations in condensed matter and the "bond lattice". Model for the liquid-glass transition. *J. Chem. Phys.* 57 (1972) 470-481.

34. **M.I. Ojovan, K.P. Travis, and R.J. Hand.** Thermodynamic parameters of bonds in in glassy materials from viscosity temperature relationships. *J. Phys.: Cond. Matter.* 19 (2007) 415107.

35. **M.I. Ojovan, W.E. Lee.** Connectivity and glass transition in disordered oxide systems. *J. Non-Cryst. Sol.* 356 (2010) 2534-2540.

36. **M.I. Ojovan.** Ordering and structural changes at the glass-liquid transition. *J. Non-Cryst. Sol.* 382 (2013) 79.

37. **H. Sher, R. Zallen.** Critical density in percolation processes. *J. Chem. Phys.* 53 (1970) 3759-3761.

38. **M.I. Ojovan, D.V. Louzguine-Luzgin.** Revealing structural changes at glass transition via radial distribution functions. *J. Phys. Chem. B.* 124(15) (2020) 3186-3194.

39. **J. Souletie and J.L. Tholence.** Critical slowing down in spin glasses and other glasses: Fulcher versus power law. *Phys. Rev.* B32 (1985) 516-519.

40. **R. Rammal and A. Benoit.** Critical Ising spin dynamics near the percolation threshold. 55 (1985) 649-652.

41. **C.L. Henley.** Critical Ising spin dynamics on percolation clusters. *Phys. REv.. Lett.* 54 (1985) 2030-2033.

42. **D.S. Sanditov, M.I. Ojovan, M.V. Darmaev.** Glass transition criterion and plastic deformation of glass. *Physica B.* 582 (2020) 411914.

43. **J. Souletie.** The glass transition: dynamic and static scaling approach. *J. Phys. France.* 51 (1990) 883-898.

44. **G. Wilde, I.R. Lu, R. Willnecker.** Fragility, thermodynamic properties, and thermal stability of Pd-rich glass forming liquids. *Mater. Sci. Eng.* A375-377 (2004) 417-421.

45. **N.O. Birge and S.R. Nagel.** Specific-heat of the glass transition. *Phys. Rev. Lett.* 54 (1985) 2674-2677.

46. **N.O. Birge.** Specific-heat spectroscopy of glycerol and propylene glycol near the glass transition. *Phys. Rev. B.* 34(3) (1986) 1631-1642.

47. **C. Hohenberg, and B.I. Halperin.** Theory of dynamic critical phenomena. *Rev. Mod. Phys.* 49 (1977) 435.

48. **M. Mozurkevitch, S. Benson.** Negative activation energies and curved Arrhenius plots: 1- theory of reaction over potential wells. *J. Phys. Chem.* 88 (1984) 6429-6435.

49. **C. Alba, L.E. Busse, D.J. List, and C.A. Angell.** Thermodynamic aspects of the vitrification of toluene, and xylene isomers, and the fragility of liquid hydrocarbons. *J. Chem. Phys.* 92 (1990) 617-624.

50. **C. Alba-Simonesco, J. Fan, and C.A. Angell.** Thermodynamic aspects of the glass transition phenomenon. II. Molecular liquids with variable interactions. *J. Chem. Phys.* 110 (1999) 5262-5271.

51. **M. Hassaine, R.J. Jimenez-Rioboo, I.V. Sharapova, O.A. Korolynk, A.I. Krivchikov, and M.A. Ramos.** Thermal properties and Brillouin-scattering study of glass, crystal, and "glacial" states in n-butanol. *J. Chem. Phys.*131 (2009) 174508.

52. **A. Mandanici, M. Cutroni, A. Triolo, V. Rodriguez-Mora, and M.A. Ramos.** Thermodynamic study of alkyl-cyclohexanes on liquid, glassy, and crystalline states. *J. Chem. Phys.* 125 (2006) 054514.

53. **S. Takahura, O. Yamamuro, H. Suga.** Heat capacities and glass transitions of 1-propanol and 3-methylpentane under pressure. new evidence for the entropy theory. *J. Non-Cryst. Sol.* 171 (1994) 259-270.

54. **S.L. Shamblin, X. Tang, L. Chang, B.C. Hancock and M.J. Pickal.** Characterization of the time scales of molecular motion pharmatically important glasses. *J. Phys. Chem B.* 103 (1999) 4113-4121.

55. **G.J. Fan, H. Choo, P.K. Liaw.** Fragility of metallic glass-forming liquids: A simple thermodynamic connection. *J. Non-Cryst. sol.* 35 (2005) 3879-3883.

56. **D.V. Louzguine-Luzgin, I. Seki, S.V. Ketov, L.V. Louzguina-Luzgina, V.L. Polkin, N. Chen, H. Fecht, A.N. Vasiliev, H. Kawaji.** Glass-transition process in an Au-based metallic glass, *J. Non-Cryst. Sol.* 419 2015) 12-15.

57. **I.R. Lu, G.P. Görler, H-J Fecht, R. Willnecker.** Investigation of specific heat and thermal expansion in the glass-transition regime of Pd-based metallic glasses. *J. Non-Cryst. Sol.* 274 (2000) 294-300.

58. **B. Wunderlich.** Study of the change in specific heat of monomeric and polymeric glasses during the glass transition. *J. Phys. Chem.* 64 (1960) 1952.

59. **M. Kobayashi, and H. Tanaka.** The reversibility and first-order nature of liquid-liquid transition in a molecular liquid. *Nature Comm.*7 (2016) 13438.

60. **S. Albert, Th. Bauer, M. Michl, G. Biroli, J.-P. Bouchaud, A. Loidl, P. Luckenheimer, R. Tourbot, C. Wiertel-Gasquet, F. Ladieu.** Fifth-order susceptibility unveilqs growth of thermodynamic amorphous order in glass-formers. *Science.* 352 (2016) 1308-1311.

61. **D. Ma, A.D. Stoica, and X.L. Wang.** Power law scaling and fractal nature of medium-range order in metallic glasses. *Nature Mat.* 8 (2005) 30-34.

62. **R.F Tournier.** Thermodynamic origin of the vitreous transition. *Materials.*. 4 (2011) 869-892.

63. **G. Kurtuldu, K.F. Shamlaye, and J. Loffler.** Metastable quasi-crystal-induced nucleation in a bulk glass-forming melt. *PNAS.*115(24) (2018) 6123-6128.

64. **I. Gallino, D. Cangialosi, Z. Evenson, L. Schmitt, S. Hechler, M. Stolpe, B. Ruta.** Hierarchical aging and reversible fragile-to-strong transition upon annealing of a metallic glass former. *Acta Mater.* 144 (2018) 400-410.

65. **S. Hechler, B. Ruta, M. Stolpe, E. Pineda, Z. Evenson, O. Gross, A. Bernasconi, R. Busch, and I. Gallino.** Microscopic eviedence of the connection between liquid-liquid transition and dynamical crossover on an ultraviscous metallic glass former. *Phys. Rev. Mater.* 2 (2018) 085603.

66. **J. Schroers, B. Lohwongwatana, W.L. Johnson, A. Pekar.** Gold based bulk metallic glass. *App. Phys. Lett.* 87 (2005) 061912.

67. **J. Schroers, B. Lohwongwatana, W.L. Johnson, A. Peker.** Precious bulk metallic glasses for jewelry applications. *Mater. Sc. Eng.* A 449-451 (2007) 235-238.

68. **D.V. Louzguine-Luzgin, I. Seki, T. Yamamoto, H. Kawaji, C. Suryanarayana, and A. Inoue.** Double-stage glass transition in a metallic glass. *Phys. Rev. B.* 81 (2010) 144-202.

69. **S.H. Zhou, J. Schmid, F. Sommer.** Thermodynamic properties of liquid, undercooled liquid and amorphous Al-Cu-Zr and Al-Cu-Ni-Zr. *Thermochim. Acta.* 339 (1999) 1-9.

70. **S. Kuchemann, G. Gibbins, J. Corkerton, E. Brug, J. Ruebsam, K. Samwer.** From ultrafast to slow: Heating rate dependence of the glass transition temperature in metallic systems. *Phil. Mag. Lett.* 96(12) (2016) 454-460.

71. **C.A. Angell.** Entropy and fragility in supercooling liquids. *J. Res. Nat. Inst. Stand. Tech.* 102 (1997) 171-185.

72. **A. Raemy, T.F. Schweizer.** Thermal behaviour of carbohydrates studied by heat flow calorimetry. *J. Therm. Anal.* 28 (1983) 95-108.

73. **Gangasharan and S.S.N. Murthy.** Nature of the relaxation process in the supercooled liquid and glassy states of some glassy carbohydrates. *J. Phys. Chem.* 99 (1995) 12349-12354.

74. **B.C. Hancock, M. Parks.** What is the true solubility advantage for amorphous pharmaceuticals. *Pharma. Res.* 17 (2000) 397-403.

75. **Y. Aso, S. Yoshioka, S. Kojima.** Relationship between the crystallization of amorphous nifedipine, phenobarbital and flopropione, and their molecular mobility as measured by their enthalpy relaxation and (1)H NMR relaxations. *J. Pharm. Sci.* 59 (2000) 408-416.

76. **L.M. Wang, C.A. Angell, R. Richert.** Fragility and thermodynamics in nonpolymeric glass-forming melts. *J. Chem. Phys.* 125 (2006) 074505.

77. **I. Tsukushi, O. Yamamuro, T. Ohta, T. Matsuo, H. Nakano, and Y. Shinota.** A calorimetric study of the configurational enthalpy and low-energyexcitation of ground amorphous solid and liquid-quenched glass of 1,3,5-tri-α-naphtylbenzene. *J. Phys. Cond. Mat.* 8 (1996) 245.

78. **K. Kishimoto, H. Suga, and S. Seki.** Calorimetric study of the glass state.VIII....of isopropylbenzene. *Bull. Chem. Soc. Jpn.*46 (1973) 3020-3031.

79. **H. Finke and J. Messerly.** 3-methylpentane and 3-methylheptane; low temperatures thermodynamic properties. *J. Chem. Therm.* 5 (1973) 247-257.

80. **L. Carpentier, S. Desprez, and M. Descamps.** Crystallization and glass properties of pentitols Xylitol, adonitol, arabitol. *J. Therm. Analys. Calor.* 73 (2003) 577-586.

81. **L.M. Wang, V. Velikov, and C.A. Angell.** Direct determination of kinetic fragility indices of glass forming liquids by differential scanning calorimetry: kinetic versus thermodynamic fragilities. *J. Chem. Phys.* 117 (2002) 10184.

82. **S.S.N. Murthy, A. Pakairay,N. Arya.** Molecular relaxation and excess of entropy in liquids and their connection to the structure of glass. *J. Chem. Phys.* 10 (1995) 8213-8220.

83. **J.E. Kunzler, W.F. Giauque.** The heat capacity and entropy of sulfuric and trihydrate glass and crystals from 15 to 300°K. *J. Chem. Therm.* 74 (1952) 797-800.

84. **K.D. Beyer, A.R. Hansen, and M. Poston.** The search for sulfuric and octahydrate: experimental evidence. *J. Chem. Phys.* 107 (2003) 2025-2032.

85. **S.S. Chang, J.A. Horman, B.A. Bestul.** Heat capacities and related thermal data for diethylphtalate crystal, glass, and liquid to 360 K. *J. Res. Natl. Bur. Stand.* 71 (1967) 293-305.

86. **D. Huang, G.B. McKenna.** New insights into the fragility dilemma in liquids. *J. Chem. Phys.* 114 (2001) 5621-5630.

87. **S. Takahara, O. Yamamuro, and T. Matsuo.** Calorimetric study of 3-bromopenthane: correlation between structural relaxation time and configurational entropy. *J. Phys. Chem.* 99 (1995) 9589-9592.

88. **M. Mizukami, H. Fujimori, and M. Oguni.** Glass transitions andthe responsible molecular motions in 2-methyltetrahydrofuran. *Prog. Theor. Phys. Suppl.* 126 (1997) 79-82.

89. **K. Takeda, O. Yamamuro, and H. Suga.** Thermodynamic study of 1-butene. Exothermic and endothermic enthalpy relaxations near the glass transition. *J. Phys. Chem. Sol.* 1991, Vol. 52(4), pp. 607-615.

90. **J.G. Aston, H.L. Fink, A.B. Bestul, A.L. Pace, and G.L. Szasz.** The heat capacity and entropy, heats of fusion and vaporization and vapor-pressure of 1-butene. *J. Am. Soc.* 68 (1946) 52-62.

91. **O. Yamamuro, I. Tsukushi, A. Lindquist, S. Takahara, M. Ishikawa, and T. Matsuo.** Calorimetric study of glassy and liquid toluene and ethylbenzene: Thermodynamic approach to spatial heterogeneity in glass-forming molecular liquids. *J. Chem. Phys.* 102 (1998) 1605-1609.

92. **D.R. Douslin, H.F. Huffman.** Low temperature thermal data on the five isometric hexanes. *J. Am. Chem Soc.* 68 (1946) 1704-1708.

93. **S. Takahara, O. Yamamuro, H. Suga.** Heat capacities and glass transitions of 1-propanol and 3-methylpentane under pressure. *J. Non-Cryst. Sol.* 171 (1994) 259-270.

94. **J.F. Counsell, E.B. Lees, J.F. Martin.** Thermodynamic properties of organic ...2-methylpropanol and pentanol. *J. Am.Chem. Soc.* 8 (1968) 1819-1823.

95. **P. Richet, Y. Bottinga.** Thermochemical properties of silicate glassesv and liquids. *Rev. Geophys.* 24(1) (1986) 1-25.

96. **L. Kosa, K. Adamkovicova, I. Prok.** Determining the heat of incongruent decomposition of merwinite. *Silikaty Prague.* 25 (1981) 199-206.

97. **D.F. Weil, J.F. Stebbins, R. Hon, I.S.E. Carmichael.** The enthalpy of fusion of of anorthite. *Contr. Mineral. Petrol.* 74 (1980) 95-102.

98. **F. Gronvold.** Heat capacities and thermodynamic properties of hexagonal and liquid selenium in the range 298 to 1000 K: enthalpy and temperature of fusion. *J. Chem. Thermodyn.* 5 (1973) 525-531.

99. **S.S. Chang and A.B. Bestul.** Heat capacities of selenium crystal (trigonal), glass and liquid from 5 to 360 K. *J. Chem. Thermodyn.* 6 (1974) 325-344.

100. **J.F. Stebbins, I.S.E. Carmichael, and L.K. Moret.** Heat capacities and entropies of silicate liquids and glasses. *Contr. Mineral. Petrol.* 86(1984) 131-148.

101. **H. Hikawa, M. Oguni, and H. Suga.** Construction of an adiabatic calorimeter for a vapor deposited sample and thermal characterization of amorphous butyronitrile. *J. Non-Cryst. Sol. 101 (1988)* 90-100.

102. **M. Oguni, H. Hikawa, and H. Suga.** Enthalpy relaxation in vapo-deposited butyronitrile. *Therm. Chim. Act.* 158 (1990) 143-56.

103. **K. Naito, A. Mura.** Molecular designfor nonpolymeric organic dye glasses with thermal stability: relations between thermodynamic parameters and amorphous properties. *J. Phys. Chem.* 97 (1993) 6240-6248.

104. **H.G. Carlson, and E.F. Westrum.** Methanol: heat capacity, enthalpies of transitions and melting, and thermodynamic properties from 5-300 K. *J. Phys. Chem.* 54 (1971) 1464-1471.

105. **O. Haida, H. Suga, and S. Seki.** Calorimetric study of the glassy state. XII. Plural glass-transition phenomena of ethanol. *J. Chem. Therm.* 9 (1970) 1133-1148.

106. **I-R Lu, G. Wilde, G.P. Gorler.** Thermodynamic properties of Pd-based glass-forming alloys. *J. Non-Cryst. Sol.* 250-252 (1990) 577-581.

107. **N. Nishiyama, M. Horino, O. Haruyama, and A. Inoue.** Abrupt change in heat capacity of supercooled PdCuNiP melt during continuous cooling. *Mater. Sci. Eng.* A304-306 (2001) 683-686.

108. **G.J. Fan, J.F Löffler, R.K. Wunderlich, H-J Fecht.** Thermodynamics, enthalpy relaxation and fragility of the bulk metallic glass-forming liquid $Pd_{43}Ni_{10}Cu_{27}P_{20}$. 52 (2004) 667-674.

109. **G. Wilde, G.P. Görler, R. Willnecker, G. Dietz.** The thermodynamic properties of $Pd_{40}Ni_{40}P_{20}$ in the glassy, liquid, and crystalline states. *Appl. Phys. Lett.* 65(4) (1994) 397-399.

110. **J. Schroers.** On the formability of bulk metallic glass in its supercooled liquid state. *Acta Mater.* 56 (2008) 471-478.

111. **I. Gallino, M.B. Shah, R. Busch.** Enthalpy relaxation and its relation to the thermodynamics and crystallization of the $Zr_{58.5}Cu_{15.6}Ni_{12.8}Al_{10.3}Nb_{2.8}$. *Acta Mater.*55 (2007) 1367-1376.

112. **H.S. Chen.** A method for evaluating viscosities of metallic glasses from the rates of thermal transformations. *J. Non-Cryst. Sol.* 27 (1978) 257-263.

113. **Q.K. Jian, X.D. Wang, X.P. Nie, G.Q. Zhang, H. Ma, H.J. Fecht, J. Bendnarck, H. Franz, Y.G. Liu, Q.P. Cao, J.Z. Jiang.** Zr-(Cu,Ag)-Al bulk metallic glasses. *Acta Mater.* 56 (2008) 1785-1796.

114. **Q.K. Zhang, H. Hahn.** Study of the kinticsof free volume in $Zr_{45}Cu_{39.3}Al_{17}Ag_{8.7}$ Bulk metallic glasses during isothermal relaxation by enthalpy experiments. *J. Non-Cryst. Sol.* 355 (2009) 2616-2621.

115. **S.C. Glade and W.L. Johnson.** Viscous flow of the $Cu_{47}Ti34Zr_{11}Ni_8$ glass gforming alloy. *J. Appl. Phys.*87(10) (2000) 7249-7251.

116. **S.C. Glade, R. Busch, D.S. Lee, W.L. Johnson, R.K. Wunderlich, and H. Fecht.** Thermodynamics of $Cu_{47}Ti_{34}Zr_{11Ni8}$, $Zr_{52.5}Cu_{17.9}Ni_{14.6}Al_{10}Ti_5$ and $Zr_{57}Cu_{15.4}Ni_{12.6}Al_{10}Nb_5$. *J. Appl. Phys.* 87 (2000) 7242-7248.

117. **M. Frey, R. Busch, W. Possart, I. Gallino.** On the thermodynamic, kinetics and sub-T_g relaxation of Mg-based bulk metallic glasses. *Acta Mater.* 155 (2018) 117-127.

118. **F. Sommer.** Thermodynamics of liquid alloys. *Mater. Sci. Eng.* A226-228 (1997) 757-762.

119. **Z.P. Lu, Y. Li, C.T. Liu.** Glass-forming tendency of bulk La-Al-Ni-Cu-(Co) metallic glass-forming melt. *J. Appl. Phys.* 93(1) (2003) 286-290.

120. **Z.P. Lu, X. Hu, Y. Li.** Thermodynamics of La based La-Al-Cu-Ni-(Co) alloys studied by temperature modulated DSC. *Intermetallics.* 8 (2000) 477-480.

121. **A. Sipp, Y. Bottinga, P. Richet.** New high viscosity data for 3D network liquid and new correlations between old parameters. *J. Non-Cryst. Sol.* 288 (2001) 166-174.

122. **J. Wong, C.A. Angell,.** *Glass structure by spectroscopy.* New York : Marcel Dekker, 1976. p. 876.

123. **A.I. Krivchikov, M. Hassaine, I.V. Sharapova, O.A. Korolyuk, R.J. Jimenez-Rioboo,M.A. Ramos.** Low temperature properties of glassy and crystalline states of n-butanol. *J. Non-Cryst. Sol.* 357 (2011) 524-529.

124. **R. Kurita, and H. Tanaka.** On the abundance and general nature of the liquid-liquid phase transition in molecular systems. *J. Phys.: Condens. Matter.* 17 (2005) L293-L302.

125. **A. Hedoux, Y. Guinet, L. Paccou, P. Derollez, and F. Danede.** Vibrational and structural properties of amorphous n-butanol: a complementary Raman spectroscopy and X-ray diffraction study.138 (2013) 214506.

126. **C.T. Moynihan, and S. Cantor.** Viscosity and its temperature dependence in molten BeF_2. *J. Chem. Phys.* 48 (1968) 115-119.

127. **D. Cangialosi, V.M. Boucher, A. Alegria, and J. Colmenero.** Direct evidence of two equilibrium mechanisms in glass polymers. *Phys. Rev. Lett.* 111 (2013) 095701.

128. **V.M. Boucher, D. Cangialosi, A. Alegria, and J. Colmenero.** Enthalpy recovery of glassy polymers: Dramatic deviations from the extrapolated liquidlike behavior. *Macromolecules.* 44 (2011) 8333-8342.

129. **R.C. Welch, J.R. Smith, M. Potuzak, X. Guo, B.F. Bowden, T.J. Kiczenski, D.C. Allan, E.A. King, A.J. Ellison, and J.C. Mauro.** Dynamics of Glass relaxation at room temperature. *Phys. Rev. Lett.* 110 (2013) 265901.

130. **L. Andreozzi, M. Faetti, M. Giordano, and F. Zulli.** Molecular-weight dependence of enthalpy relaxation of PMMA. *Macromolecules. 3*8 (2005) 6056-6067.

131. **J.M.G. Cowie, S. Harris, I.J. McEwen.** Polymer aging in poly(vinyl acetate) 1. Enthalpy relaxation. *J. Polymer Sci. part B, Polym. Phys.* 35(7) (1998) 1107-1116.

132. **E.-A. McGonicle, J.M.G. Cowie, V. Arrighi, R.A. Pethrick.** Enthalpy relaxation and free volume changes in aged styrene copolymers containing a hydrogen bonding co-monomer. *J. Mater. Sci.* 40 (2005) 1869-1881.

133. **H. Jabroui, S. Ouaskit, J. Richard, J-L. Garden.** Determination of entropy production during glass transition: theory and experiment. *J. Non-Cryst. Sol.* 533 (2020) 119907.

134. **N. Brun, P. Bourson, S. Margueron, M. Duc.** Study of the thermal behavior of syndiotactic and atactic polystyrene by Raman spectroscopy. *Jeep.* 2001. published by EDP Sciences.
DOI: 10.1051/jeep/201100004

135. **M.S. Beasley, M. Tylinski, Y.Z. Chua, C. Schick, and M.D. Ediger.** Glasses of three alkyl phosphates show a range of kinetic stabilities when prepared by physical vapor deposition. *J. Chem. Phys.* 148 (2018) 174503.

136. **M. Tylinski, Y.Z. Chua, M.S. Beasley, and M.D. Ediger.** Vapor-deposited alcohol glasses reveal a wide-range of kinetic stability. *J. Chem. Phys.* 145 (2016) 174506.

137. **J.Q. Wang, Y. Shen, J.H. Perepezko, M.D. Ediger.** Increasing the kinetic stability of bulk metallic glasses. *Acta Mater.* 104 (2016) 25-32.

138. **M. Ahrenberg, Y.Z. Chua, R. Whitaker, H. Huth, M.D. Ediger and C. Schick.** *In situ* investigation of vapor-deposited glasses of toluene and ethylbenzene via alternating current chip-nanocalorimetry. *J. Chem. Phys.* 138 (2013) 024501.

139. **S.L.L.M. Ramos, M. Oguni, K. Ischii, and H. Nakayama.** Character of devitrification, viewed from enthalpic paths, of the vapor-deposited ethylbenzene glasses. *J. Phys. Chem. B.* 115 (2011) 14327-14332.

140. **H.-B. Yu, Y. Luo, and K. Samwer.** Ultrastable metallic glass. *Adv. Mater.* 25 (2013) 5904-5908.

141. **K.L. Kearns, K.R. Whiteker,M.D. Ediger,H. Huth, and C. Schick.** Observation of low heat capacities for vapor-deposited glasses of indomethacin as determined by AC nanocalorimetry. *J. Chem. Phys.* 133 (2010) 014702.

142. **K.L. Kearns, S.F. Swallen, and M.D. Ediger, T. Wu , Y. Sun, L. Yu.** Hiking down the energy landscape: Progress toward the Kauzmann temperature via vapor deposition. *J. Phys. Chem. B.* 112 (2008) 4934-4942.

143. **K.L. Kearns, S.F. Swallen, and M.D. Ediger, T. Wu and L. Yu.** Influence of substrate temperature on the stability of glasses prepared by vapor deposition. *J. Chem. Phys.* 2007, Vol. 127, p. 154702.

144. **K. R. Whiteker, D. J. Scifo, M.D. Ediger, M. Ahrenberg, and C. Schick.** High stable glasses of Cis-decalin and cis/rans-decalin mixtures. *J. Phys. Chem.* 117 (2013) 12724-12733.

145. **K. R. Whiteker, M. Tylinski, M. Ahrenberg, C. Schick, and M.D. Ediger.** Kinetic stability and heat capacity og vapor-deposited glass of o-terphenyl. *J. Chem. Phys.* 143 (2015) 084511.

146. **Y. Z. Chua, M. Ahrenberg, M. Tylinski, M. D. Ediger, and C. Schick.** How much time is needed to form a kinetically stable glass? Ac calorimetric study of vapor-deposited glasses of ethylcyclohexane. *J. Chem. Phys.* 142 (2015) 054506.

147. **K. Takeda, O. Yamamuro, I. Tsukushi, T. Maysuo, and H. Suga.** Calorimetric study of ethylene glycol and 1-3-propadeniol: configuratinal entropy in supercooled polyalcohols. *J. Mol. struct.* 479 (1999) 227-235.

148. **E. Leon-Gutierrez, A. Sepulveda, G. Garcia, M. T. Clavaguera-Mora and J. Rodriguez-Viejo.** Stability of thin film glasses of toluene and ethylbenzene formed by vapor deposition: an in situ nanocalorimetric study. *Phys. Chem. Chem. Phys.* 12 (2010) 14693-14698.

149. **D. Battacharya, and V. Sadtchenko.** Enthalpy and high temperature relaxation kinetics of stable vapor-deposited glass of toluene. *J. Chem. Phys.*141 (2014) 094502.